Dilepton production by dynamical quasi-particles in the strongly interacting quarkgluon plasma

O Linnyk

Dilepton production by dynamical quasiparticles in the strongly interacting quark-gluon plasma

O. Linnyk

Institut für Theoretische Physik, Johann Wolfgang Goethe University,
Ruth-Moufang-Str. 1, 60438 Frankfurt am Main, Germany

E-mail: linnyk@fias.uni-frankfurt.de

Abstract. We address the dilepton production by the constituents of the strongly interacting quark-gluon plasma (sQGP). In order to make quantitative predictions for dilepton rates at experimentally relevant low dilepton mass ($O(1$ GeV$)$) and strong coupling ($\alpha_S \sim 0.5 \div 1$), we take into account non-perturbative spectral functions and self-energies of the quarks, anti-quarks and gluons. For this purpose, we use parametrizations of the quark and gluon propagators provided by the dynamical quasiparticle model (DQPM) matched to reproduce lattice QCD data. The DQPM describes QCD properties in terms of single-particle Green's functions and leads to the notion of the constituents of the sQGP being effective quasiparticles, which are massive and have broad spectral functions (due to large interaction rates). By "dressing" the quark and gluon lines with the effective propagators, we derive the off-shell cross sections for dilepton production in the reactions $q + \bar{q} \to l^+l^-$ (Born mechanism), $q + \bar{q} \to g + l^+l^-$ (quark annihilation with the gluon Bremsstrahlung in the final state), $q(\bar{q}) + g \to q(\bar{q}) + l^+l^-$ (gluon Compton scattering), $g \to q + \bar{q} + l^+l^-$ and $q(\bar{q}) \to q(\bar{q}) + g + l^+l^-$ (virtual gluon decay, virtual quark decay). In contrast to previous calculations of these cross sections, we account for virtualities of all the quarks and gluons. We find that finite masses of the effective quasiparticles not only screen the singularities typical to the perturbative cross sections with massless quarks, but also modify the shape of the dilepton production cross sections, especially at low dilepton mass Q and at the edges of the phase space. Finally, we use the calculated mass-dependent cross sections to identify the dependence of the dilepton rates on the spectral function *widths* of the initial and final quarks and gluons, which has not been estimated so far. The results demonstrate that the multiple partonic scatterings encoded in the broad spectral functions of the dynamical quasiparticles have considerable effect on the dilepton rates.

1. Introduction

Since many years the transition between the hadronic phase and the quark-gluon plasma (QGP) as well as the nonperturbative properties of the QGP motivate a large community and justify large-scale experiments, in which heavy nuclei are collided at relativistic energies in order to achieve the high energy densities necessary for the transition to the deconfined state of matter. Electromagnetic probes (i.e. dileptons and photons) are powerful tools to explore the early (hot and dense) stage of the heavy-ion collision, since, unaffected by the final state interaction, they carry to the detector information about the conditions and properties of the environment at the time of their production – encoded in their mass and momentum distributions, – thus providing a glimpse deep into the bulk of the strongly interacting matter [1, 2]. In 1978, E. Shuryak proposed to use dileptons as probes of QGP, after the suggestion was made that the dilepton and photon yields reflect the properties of the medium created in hadron-hadron collisions (see the pioneering works [3, 4, 5, 6, 7]).

Real and virtual photons, i.e. dileptons, are emitted over the entire space-time evolution of the heavy-ion collision, from the initial nucleon-nucleon collisions through the hot and dense phase and to the hadron decays after freeze-out. This is both a challenge and advantage of electromagnetic probes. Fortunately, lepton pairs possess an additional degree of freedom (the invariant mass Q^2), which allows to separate different "physics" by observing the dilepton radiation in different mass ranges. The low mass ($Q < 1$ GeV) spectrum of dileptons – generated in heavy ion collisions – is dominated by the vector meson decays, the production of lepton pairs of high mass ($Q > 3$ GeV) is governed by the perturbative quantum chromodynamics (pQCD), while the dilepton yield in the intermediate mass range ($1 < Q < 3$ GeV) is sensitive to the possible formation of a QGP [8].

Dilepton measurements have possibly provided a signal of the deconfined matter at SPS energies. The NA60 Collaboration [9, 10, 11] has recently found that the effective temperature of the dileptons in the intermediate mass range is lower than the $T_{\rm eff}$ of dileptons at lower masses, which are of hadronic origin. This can be explained, if one assumes that the spectrum at the invariant masses above 1 GeV is dominated by the partonic channels in the QGP [12, 13, 14]. In this case, the softening of the transverse mass spectrum with growing invariant mass implies that the partonic channels occur dominantly before the collective radial flow has developed. The assumption that the dilepton spectrum at masses above 1 GeV could be dominated by QGP radiation was supported by the studies within the Hadron-String-Dynamics (HSD) transport approach [15]. While it was shown [16] that the measured dilepton yield at low masses ($Q \leq 1$ GeV) can be explained by the dilepton production in the hadron interaction and decay, there is a discrepancy between the HSD results and the data in the mass range above 1 GeV. This access seen at $Q > 1$ GeV is not accounted for by hadronic sources in HSD – in-medium or free – and might be seen as a signal of partonic matter,

manifest already at 158 AGeV incident energy.

Recently, the PHENIX Collaboration has presented first dilepton data from pp and $Au + Au$ collisions at Relativistic Heavy Ion Collider (RHIC) energies of $\sqrt{s} =$ 200 GeV [17, 18, 19, 20]. The data show a large enhancement over hadronic sources [21] in $Au + Au$ reactions in the invariant mass regime from 0.15 to 0.6 GeV and from 1 to 3 GeV, which could not be explained in the scope of the HSD approach neither by meson decays – in-medium or free – nor by hadronic Bremsstrahlung [16]. It is of interest, whether the excess at RHIC is due to the dominance of sources in the QGP.

First concepts of the QGP were guided by the idea of a system of partons which interact weakly, with pQCD cross sections. Consequently, early predictions of the dilepton emission from QGP relied on perturbative formulae for the cross sections of the virtual photon production in $q + \bar{q}$ and $q + g$ collisions [4, 22, 23]. Due to large running coupling, the next-to-leading order (NLO) gluon-quark interactions contribute considerably in addition to the leading order (Born) mechanism of quark-quark annihilation ($q\bar{q} \rightarrow l^+l^-$) to the QGP radiation spectrum [24]. While the effect of multiple scattering of the quark in the plasma (Landau-Pomeranchuk-Migdal effect [25, 26, 27]) on the rate of $q\bar{q} \rightarrow \gamma^*$ was stressed in [28].

Not long ago, a first attempt was made to calculate directly on the lattice the production of dileptons in the QGP [29]. The suppression at small Q^2 observed on the lattice has attracted a lot of interest, because it is not what one would expect from perturbation theory: The finite thermal masses would indeed produce a drop of the Born term $q + \bar{q} \rightarrow \gamma^*$ because of the threshold effect – as predicted [30] in relation to the cut-off in the momentum distribution of quarks and confirmed in effective perturbation theory in the works [31, 32, 33], – but there are higher order processes ($q\bar{q} \rightarrow \gamma^* g$, $qg \rightarrow \gamma^* q$) that have no threshold and would fill the spectrum at small Q^2. Also, the rescattering effects can lead to the disappearance of the threshold behavior in the Born ($q\bar{q} \rightarrow \gamma^*$) rate [28].

Recent theoretical and experimental works have shown that the QGP as produced in heavy-ion collisions is a strongly interacting many-body system. Indeed, most theoretical estimates of the temperatures, which are reasonably expected to be currently achieved in heavy-ion collisions are not extremely large compared to the QCD scale Λ_{QCD} [34]. In agreement with this expectation, experimental observations at RHIC indicated that the new medium created in ultra-relativistic Au+Au collisions was interacting strongly – even stronger than hadronic matter. Moreover, in line with theoretical studies in Refs. [35, 36, 37] the medium showed phenomena of an almost perfect liquid of partons [38, 39, 40, 41] as extracted from the strong radial expansion and elliptic flow of hadrons [38, 39, 40, 41]. Studies performed in the framework of lattice QCD [42] have also shown that the high temperature plasma phase is a medium of interacting partons which are strongly screened and influenced by nonperturbative effects even at temperatures as high as $10\,T_c$. Consequently, the concept of perturbatively interacting quarks and gluons as constituents of the QGP had to be reconsidered. Thus one is forced to go beyond pQCD in calculating dilepton production

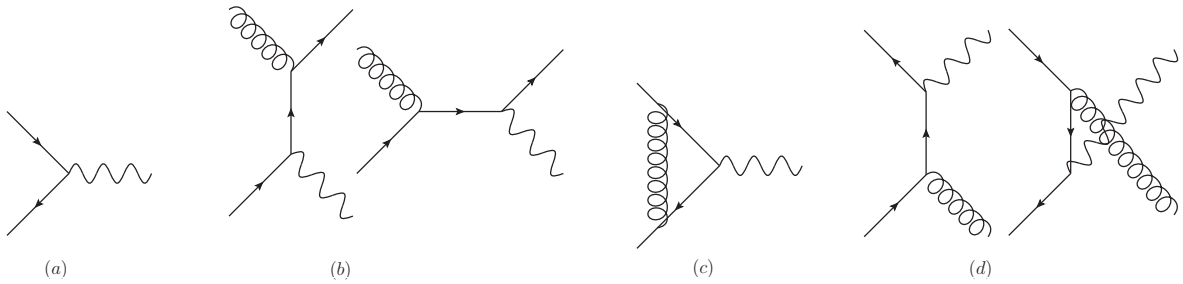

Figure 1. Perturbative QCD diagrams contributing to the dilepton production up to the order $O(\alpha_S)$: (a) Drell-Yan mechanism, (b) gluon Compton scattering (GCS), (c) vertex correction, (d) quark annihilation with gluon Bremsstrahlung. Virtual photons (wavy lines) split into lepton pairs, spiral lines denote gluons, arrows denote quarks. In each diagram, the time runs from left to right.

in the strongly interacting QGP.

To some degree a solution can be found in reordering perturbation theory: by expanding correlation functions in terms of effective propagators and vertices instead of bare ones [43]. A powerful resummation technique was developed by Braaten, Pisarsky [44] and Wong [45]. The production of dileptons was calculated at leading order in the effective perturbation expansion in [44], using as the effective propagators the bare ones plus one loop corrections evaluated in the high-temperature limit [46, 47, 48, 49]. In this approach the singularity of the production cross section – that dominates the dilepton rate – is regularized by the thermal masses of quarks m_{th} and gluons m_g, which are in turn determined by the one-loop leading order result in the thermal perturbation theory (HTL). The approach has been extended to the dilepton radiation from non-equilibrium plasmas in [50, 51].

On the other hand, the nonperturbative nature of the sQGP constituents manifests itself in their strong coupling, multiple scattering and modified spectral densities and self energies. In order to take *all* these phenomena into account in the calculation of dilepton production from the QGP, we refrain from a fixed order thermal loop calculation relying on perturbative self-energies (calculated in the limit of infinite temperature) to fix the in-medium masses of the quarks and gluons and pursue instead a phenomenological approach. Indeed, since virtual photon rates need to be evaluated at temperatures that are not very large compared to T_c, it is advisable to adopt values for m_{th}, m_g not from the HTL approximation. Possible alternative strategies are: (i) to treat the thermal masses in the calculation of the dilepton rates as phenomenological parameters as in [33] or (ii) to obtain them from fits of the lattice QCD entropy by an equation of state corresponding to a gas of quasiparticles (massive quarks and gluons) as in Refs. [52, 53] or (iii) *dynamical* quasi-particles (massive and *broad* quarks and gluons) as in Refs. [31, 32].

In the latter approach – followed here, – the (multiple) strong interactions of quarks and gluons in the sQGP are encoded in their effective broad spectral functions. The

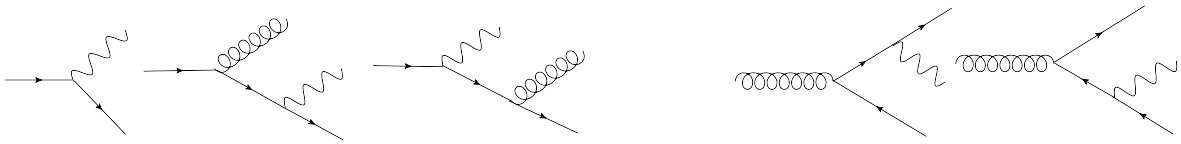

Figure 2. Diagrams contributing to the dilepton production by virtual quasi-particles in addition to the ones presented in Fig. 1. Lhs: the decay of a virtual quark; Rhs: the decay of a virtual gluon. Virtual photons (wavy lines) split into lepton pairs, spiral lines denote gluons, arrows denote quarks.

effective propagators, which are understood as resummed propagators in a hot QCD environment, have been extracted from lattice data in the scope of the Dynamical QuasiParticle Model (DQPM) in Ref. [54]. The DQPM describes QCD properties in terms of single-particle Green's functions (in the sense of a two-particle irreducible (2PI) approach) and leads to a quasi-particle equation of state, which reproduces the QCD equation of state extracted from Lattice QCD calculations. According to the DQPM, the constituents of the sQGP are strongly interacting massive partonic quasi-particles with broad spectral functions.

Let us note that we will study the dilepton production in the interaction of quarks and gluons in the sQGP, while explicitly taking into account their finite *widths*. The non-zero width of quark spectral functions reflects their strong interaction, which is manifest in the elastic scattering as well as in the virtual gluon emission. By dressing the external partonic lines in the dilepton production processes ($q + \bar{q} \to l^+l^-$, $q + \bar{q} \to g + l^+l^-$, $q+g \to q+l^+l^-$) with spectral functions we study the effect of the partonic interactions in the plasma on its dilepton radiation, especially in the interesting region of low Q^2. Certain aspects of the dilepton production by partons with finite masses have been studied in earlier works [55, 56, 33, 57, 58], but here we will extend these studies by assigning finite masses to *all* parton lines and, more importantly, by going beyond the zero width approximation for initial and finite partons. Thus we will be able to test to what extend the properties of the quark and gluon quasi-particles can be seen in the dilepton rates, e.g. due to large phase-space corrections, broad spectral function widths as well as a different dependance of the strong coupling on the temperature T of the medium.

For this purpose we first derive the off-shell cross sections of $q + \bar{q} \to l^+l^-$, $q+\bar{q} \to g+l^+l^-$, $q+g \to q+l^+l^-$ ($\bar{q}+g \to \bar{q}+l^+l^-$), $q \to q+g+l^+l^-$ ($\bar{q} \to \bar{q}+g+l^+l^-$) and $g \to q+\bar{q}+l^+l^-$ by calculating them for the arbitrary virtualities of external quarks and gluons, while dressing the internal lines with effective self energies. Consequently, we take into account the non-zero widths of initial and final state partons by convoluting the obtained cross sections with the effective spectral functions. Using the DQPM parametrizations for the quark(gluon) self-energies, spectral functions and interaction strength, we calculate the dilepton production from partonic interactions in the sQGP in the first order of electromagnetic coupling, i.e. incorporating only a single photon

line. We note that approaches very similar in spirit have been performed in the past(and present) for dilepton production in hadron-hadron reactions [59, 60, 61, 62] where the strong interaction has been parametrized to describe elastic and inelastic scattering in the leading order of perturbation theory. The dilepton production then is calculated by attaching an additional virtual photon line to each charged propagator. Gauge invariance finally is restored by appropriate terms in the effective Lagrangian density or alternative recipes. Verification of Ward identities in general for parton interaction within the DQPM model is beyond the scope of this publication and will be addressed elsewhere. For the current study, we check the gauge invariance of the final dilepton rates numerically, by varying the gauge parameter.

In the context of the hot QGP the perturbative diagrams for the dilepton production at order up to $O(\alpha_S)$ are illustrated in Fig. 1. Let us briefly summarize the differences of our phenomenological approach from the standard pQCD:

- (a) we take into account full off-shell kinematics, in particular the transverse motion and virtualities (masses) of the partons,
- (b) quark and gluon lines are dressed with nonperturbative spectral functions: the cross sections derived for arbitrary masses of all external parton lines are integrated over these virtualities weighted with spectral functions (see e.g. Refs [58, 63] for an introduction to the method); the internal lines are dressed with the real parts of the DQPM self energies,
- (c) vertices are modified compared to pQCD by replacing the perturbative coupling (that runs with the momentum transfer) with the full running coupling α_S that depends on the temperature T according to lattice data parametrization by [54], while the temperature is related to the local energy density ϵ by the lQCD equation of state. Note that close to T_c the full coupling increases with decreasing temperature much faster than the pQCD prediction.
- (d) Due to the broad width for quarks and gluons in the sQGP [31] – which is the consequence of their high interaction rate,– there are non-vanishing contributions also from the processes of the decays of virtual quarks ($q \to q+g+l^+l^-$) and gluons ($g \to q+\bar{q}+l^+l^-$), which are forbidden kinematically in pQCD (see Fig. 2).

The paper is organized as follows. The analysis of the off-shell kinematics and the calculations of the off-shell cross sections (i.e. elementary cross sections for arbitrary values of quark and gluon off-shellness) are calculated in section 3 for each of the partonic processes separately. On the other hand, in the limit of a high hard scale Q^2, the off-shell cross sections should approach the perturbative ones [64, 65]. In this spirit the off-shell cross sections are compared to the perturbative ones throughout section 3. Accordingly, we first recapitulate the corresponding pQCD results in section 2.

In Section 4 we give a simple example for an application of the off-shell cross sections derived above to the calculation of the relative contributions of different processes to the sQGP dilepton radiation rates. We point out, however, that the considerations in the current paper will probably be not detailed enough to allow for a proper description

of the hot and dense early phase of realistic heavy-ion collisions, where the sQGP is formed. A quantitative comparison to the experimental data and reliable conclusions on the relative contribution of various sources to the experimentally observed thermal dilepton spectrum [9, 10, 11, 17, 18, 19, 20] requires to account for the non-equilibrium dynamics of the heavy-ion collision in its full complexity by use of microscopic transport models, which is beyond the scope of this study. The main purpose of the current paper is to built an effective-theory approach for the derivation of the off-shell cross sections for the interaction of dynamical quasi-particles as constituents of the sQGP. The qualitative analysis of the relative importance of different processes in section 4 should be understood as an illustration of the present results rather than a quantitative prediction for the dilepton yield from heavy-ion collisions.

Section 5 is devoted to analyzing the effect of finite quark and gluon widths on the dilepton rate explicitly. In Section 6 we summarize the main results and their possible applications.

2. Dileptons from perturbative partons

In the present Section, we remind the cross sections and kinematics of the following partonic mechanisms for dilepton production in the standard pQCD:

(i) Born mechanism of quark annihilation ($q + \bar{q} \to \gamma^*$),

(ii) quark + anti-quark annihilation with gluon Bremsstrahlung in the final state ($q + \bar{q} \to g + \gamma^*$),

(iii) Gluon Compton scattering ($q + g \to \gamma^* + q$ and $\bar{q} + g \to \gamma^* + \bar{q}$).

2.1. Born term

The leading order pQCD mechanism for the dilepton production in the partonic phase is the same as for the well known Drell-Yan (DY) process [69]: quark and antiquark annihilate into a lepton pair ($q\bar{q} \to l^+l^-$), as presented by the diagram (a) in Fig 1. The leading order leading twist pQCD result for the cross section of DY dilepton production is

$$\left(\frac{d^3\hat{\sigma}(q\bar{q} \to l^+l^-)}{dQ^2 dx_F dq_T^2}\right)^{\rm DY}_{\rm on\text{-}shell} = \frac{4\pi\alpha^2 e_q^2}{9Q^4}\frac{x_1x_2}{x_1+x_2}\,(1-x_1x_2) \times \delta(q_T^2)\delta\left(Q^2 - x_1x_2S_{NN}\right)\delta\left(x_F - \frac{x_2-x_1}{1-x_1x_2}\right), \quad (1)$$

where α is the electromagnetic fine structure constant, e_q the fractional quark charge, the lepton pair has invariant mass Q^2 and transverse momentum q_T. The formula (1) is written in the collinear approximation. Generalizations to the final intrinsic transverse momentum are possible (see [58, 66, 67, 68] and references therein).

In collinear pQCD, the off-shellness, mass and transverse momentum of the annihilating quark and antiquark are neglected, and, therefore, the incoming parton momenta are simply related to the momenta of colliding nuclei as $p_{q(\bar{q})} = x_i P_A/A$. In this case, the parton momentum fractions x_1 and x_2 are related to the virtuality and x_F of the produced photon as (cf. delta-functions in (1)):

$$Q^2 = s = x_1 x_2 S_{NN}; \tag{2}$$

$$x_F = (x_2 - x_1)/(1 - x_1 x_2); \tag{3}$$

s denotes the invariant energy for the partonic process; S_{NN} – for the hadronic one; $x_F = q_z/(q_z)_{max}$; $q_z > 0$, if $x_2 > x_1$. The denominator of the x_F definition in (3) is omitted in some works, where an approximate definition $x_F \approx 2q_z/\sqrt{S_{NN}}$ is used.

The kinematical limits for this process are

$$S_{NN} \geq Q^2, \ |x_F| \leq 1, s = Q^2. \tag{4}$$

Note that in pQCD – both collinear and 'intrinsic k_T' approach – partons are bound by the on-shell condition

$$p_q^2 = E_q^2 - \vec{p}_q^{\,2} = 0$$

(where the current quark mass is negligible). In Section 3 we will depart from the on-shellness and will consider quarks and gluons as dynamical quasi-particles that can assume arbitrary values of virtualities p^2, distributed according to phenomenological spectral functions.

2.2. Gluon Bremsstrahlung

The pQCD cross section of the *gluon Bremsstrahlung* process $\bar{q}q \to g + \mu^+\mu^-$ is [70, 71]

$$\left(\frac{d^2\hat{\sigma}(q\bar{q} \to gl^+l^-)}{dQ^2 d\cos\Theta}\right)^{\rm gBr}_{\rm on\text{-}shell} = \frac{8\alpha^2 e_q^2 \alpha_S}{27Q^2}\frac{s - Q^2}{s^2\sin^2\Theta} \times \left(1 + \cos^2\Theta + 4\frac{Q^2 s}{(\hat{s} - Q^2)^2}\right), \tag{5}$$

where s is the total energy squared of the colliding partons, and Θ is the scattering angle of the outgoing lepton pair with respect to the incoming quark momentum in the quark center-of-mass system (CMS). Note that the cross section (5) can be written in terms of the Mandelstam variables s, t and u as [22]

$$\left(\frac{d^2\hat{\sigma}(q\bar{q} \to gl^+l^-)}{dQ^2 dt}\right)^{\rm gBr}_{\rm on\text{-}shell} = \frac{8\alpha^2 e_q^2 \alpha_S}{27Q^2}\frac{(t - Q^2)^2 + (u - Q^2)^2}{s^2 tu} \times \delta\left(s + t + u - Q^2\right) \tag{6}$$

$$= \frac{8\alpha^2 e_q^2 \alpha_S}{27Q^2 s^2}\left(\frac{t}{u} + \frac{u}{t} + \frac{2sQ^2}{tu}\right) \times \delta\left(s + t + u - Q^2\right), \tag{7}$$

which coincides with the QED cross section for the virtual Compton scattering up to the color factor and the crossing transformation [72]. Here we denote the momenta of the incoming quark and antiquark as p_1 and p_2, the momenta of the outgoing gluon and virtual photon as k and q, $s = (p_1 + p_2)^2$, $t = (p_1 - q)^2$, $u = (p_2 - q)^2$. The δ-function $\delta(s + u + t - Q^2)$ reflects the on-shell condition for the partons:

$$p_1^2 + p_2^2 + k^2 = 0. \tag{8}$$

The collinear divergence of the gluon Bremsstrahlung cross section for $t \to 0$ and $u \to 0$ (i.e. $\cos\Theta \to \pm 1$) is obvious; a cut-off Λ^2 on $|\cos\Theta|$ can be used in order to regularize it. Another divergence in the perturbative expression (6) is the infrared (IR) divergence for the energy of the gluon $k^0 \to 0$ due to the vanishing quark and gluon masses. Indeed, if all the partonic masses are neglected, we have in the CMS:

$$t = k^0(-\sqrt{s} + \sqrt{s}\cos\Theta_2) \to 0 \text{ at } k^0 \to 0. \tag{9}$$

These divergences (the soft and collinear ones) can be remedied by introducing a small finite gluon mass μ_{cut} (cf. the plasmon mass in [34]). Indeed, the gluon thermal mass μ plays the role of a natural cut-off in the sQGP (cf. section 3.2).

At this point, a note on the soft gluon resummation is due. In standard pQCD calculations *real* gluon emission leads to large logarithms $\log Q^2/q_T^2$ when q_T is small. Therefore, fixed order perturbation theory breaks down and the logarithms must be resummed. In the approximation of collinear soft gluons with strongly ordered transverse momenta the resummation leads to the Sudakov factor. However, the strongly k_T-ordered phase space, which ignores overall transverse momentum conservation, is not the dominant configuration at small q_T. A correct resummation of logarithms can be achieved in b-space [73, 74]. On the other hand, if the gluons have a finite thermal mass, as is realized in the DQPM model, the gluons are not real and the resummation is not necessary, since the divergence at $q_T \to 0$ is regularized.

2.3. Gluon Compton scattering

In QED, the Compton process refers to elastic scattering of a photon off a charged object, and has proven to be very important as it provided early evidence that the electromagnetic wave is quantized [75, 76]. In QCD, the corresponding process is the *gluon Compton scattering* $g + q(\bar{q}) \to q(\bar{q}) + \gamma^*$. The cross section in leading twist of pQCD [70] is given by:

$$\left(\frac{d^2\hat{\sigma}(g+q)}{dQ^2 d\cos\Theta}\right)^{\rm GCS}_{\rm on\text{-}shell} = \frac{\alpha^2 e_q^2 \alpha_S}{18Q^2}\frac{s-Q^2}{s^2(1+\cos\Theta)} \times \left\{\frac{2s}{s-Q^2} + \frac{s-Q^2}{2s}(1+\cos\Theta)^2 - \frac{2Q^2}{s}(1-\cos\Theta)\right\} \tag{10}$$

In terms of Mandelstam variables [22] it reads:

$$\left(\frac{d\hat{\sigma}(g+q)}{dQ^2 dt}\right)^{\rm GCS}_{\rm on\text{-}shell} = \frac{e_q^2\alpha^2\alpha_S}{9Q^2}\frac{s^2+t^2+2Q^2u}{-s^3t}\,\delta\left(s+t+u-Q^2\right), \tag{11}$$

which is obviously related by crossing transformation to (7).

3. Dileptons from dynamical quasi-particles

Let us now proceed to the calculation of the dilepton production by effective strongly interacting partonic quasiparticles with broad spectral functions. Dilepton radiation by the dynamical quasiparticles proceeds via the elementary processes illustrated in Figs. 1 and 2: the basic Born $q+\bar{q}$ annihilation mechanism, Gluon Compton scattering ($q+g \to \gamma^*+q$ and $\bar{q}+g \to \gamma^*+\bar{q}$), quark + anti-quark annihilation with gluon bremsstrahlung in the final state ($q+\bar{q} \to g+\gamma^*$); virtual quark and virtual gluon decays. We recall that, in leading order the 'dressed propagators' and strong coupling lead to substantial phase-space corrections; furthermore, the relative contribution of different channels is expected to change significantly as a function of Q^2 due to different kinematical thresholds.

Ultimately, we are interested in the dilepton yield of the strongly coupled quark-gluon plasma. Due to the factorization property proven in Ref. [34], the dilepton emission from the QGP – created in a heavy-ion collision – is given by the convolution of the elementary sub-process cross sections (describing quark/gluon interactions with the emission of dileptons) with the structure functions that characterize the properties and evolution of the plasma (encoded in the distribution of the quarks and gluons with different momenta and virtualities):

$$\frac{d^3\sigma^{\rm QGP}}{dQ^2dx_Fdq_T^2} = \sum_{abc}\int d\hat{s}\int_0^\infty dm_1^i\int_0^\infty dm_2^i\int_0^\infty d\mu^f\, F_{ab}(\hat{s},m_1^i,m_2^i) \times {\rm A}_c(\mu^f)\frac{d^3\hat{\sigma}_{abc}(\hat{s},m_1^i,m_2^i,\mu^f)}{dQ^2dx_Fdq_T^2}, \qquad (12)$$

where m_1^i and m_2^i are the off-shellnesses (i.e. virtualities) of the incoming partons, μ^f is the off-shellness of the outgoing parton, while the indices a,b,c denote quark, antiquark or gluon so that all the considered mechanisms are covered. The cross sections $\hat{\sigma}_{abc}(\hat{s},m^{i1},m^{i2},\mu^f)$ for the different processes for arbitrary values of parton virtualities will be calculated in the current Section. Consequently – in Sections 4 and 5 – we will integrate the elementary cross sections according to (12) over the motion of partons and over parton virtualities by employing phenomenological structure functions F_{ab} and spectral functions ${\rm A}_c(\mu^f)$.

3.1. Off-shell $q+\bar{q}$ in the Born mechanism

Let us first consider the general 'off-shell' kinematics, when the participating quarks are massive, with the masses distributed according to the spectral functions. We denote the masses of the quark and the anti-quark as m_1 and m_2. Just as in the 'on-shell' case,

the mass of the produced dilepton pair is fixed to the invariant energy of the quark-antiquark collision: $s = Q^2$. However, the kinematical limit for the minimal dilepton mass is now higher than in the massless on-shell case:

$$Q_0^2 \equiv s_0 = (m_1 + m_2 + 2m_{lept})^2 > 4m_{lept}^2, \tag{13}$$

where m_{lept} is the mass of an electron or muon. Also, the incident current changes:

$$J = \frac{1}{2}\sqrt{(k_1\cdot k_2)^2 - m_1^2 m_2^2} = \frac{1}{2}\sqrt{(s - m_1^2 - m_2^2)^2 - 4m_1^2 m_2^2},$$

compared to $J = s/2$ in the on-shell approximation.

In addition to the kinematics, the matrix element corresponding to the diagram (a) in Fig. 1 is modified in the general off-shell cases compared to the matrix element for the annihilation of massless quarks. The off-shell cross section was first addressed in [58] and reads:

$$\begin{aligned}\left(\frac{d^3\hat{\sigma}(m_1, m_2, \vec{p}_1, \vec{p}_2)}{dQ^2 dx_F dq_T^2}\right)_{off-shell}^{DY} &= \frac{\pi\alpha^2 e_q^2}{3Q^4 N_c\sqrt{(p_1\cdot p_2)^2 - m_1^2 m_2^2}} \\ &\times \left[2Q^4 - Q^2\left(m_1^2 - 6m_1 m_2 + m_2^2\right) - \left(m_1^2 - m_2^2\right)^2\right] \\ &\times \delta\left(Q^2 - m_1^2 - m_2^2 - 2(p_1\cdot p_2)\right) \\ &\times \delta\left(x_F - \frac{\sqrt{s_{NN}}}{s_{NN} - Q^2}\left(p_{2z} - p_{1z}\right)\right) \\ &\times \delta\left(q_T^2 - \left(\vec{p}_{1\perp} + \vec{p}_{2\perp}\right)^2\right). \end{aligned} \tag{14}$$

In (14), N_c is the number of colors, $e_q(-e_q)$ is the fractional charge of the quark (antiquark), p_i are the 4-momenta of the annihilating quark and antiquark. For $Q^2 \gg m_1^2, m_2^2$ the expression (14) reduces to the leading twist pQCD formula (the 'on-shell' approximation).

The approximation $m_1 = m_2 \to 0$ in Eq. (14) is equivalent to restricting oneself to the leading term in the twist expansion, that is, in the case of the unpolarized Drell-Yan process, an expansion in powers of $1/Q$. One can see that in this limit (and additionally using the collinear kinematics $\vec{p}_{1\perp} = \vec{p}_{2\perp} = 0$) we recover the standard pQCD result (1).

The strong interaction of partons (reflected in the self-energies) leads to higher-twist corrections to the standard pQCD cross sections [58]. The higher twists by definition are vanishing in the limit of infinite invariant mass of the lepton pair [65]. However, the power-Q^2 suppressed contributions may be large at realistic energies. For instance, quark off-shellness – arising due to the non-perturbative interaction between the partons – have an effect on the transverse momentum distribution of Drell-Yan lepton pairs in $p + \bar{p}$ collisions [57, 58, 77].

The off-shell cross sections are quantitatively compared to the leading twist results in Fig. 3. The dimuon production cross sections in the Drell-Yan mechanism are plotted in Fig. 3 (a) versus the mass of the muon pair $Q = \sqrt{s}$. The short dashes (black) line shows the on-shell, i.e. the standard perturbative result. The other lines show the

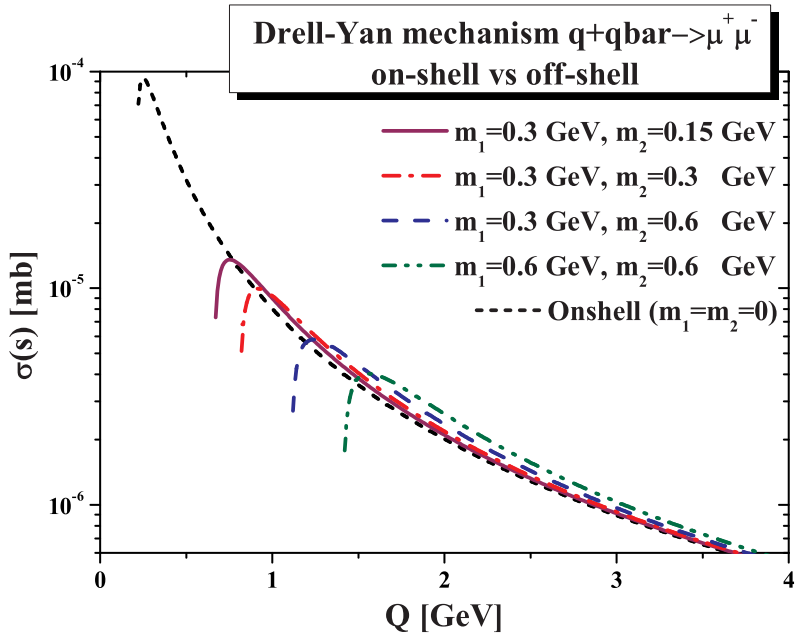

(a) Cross sections

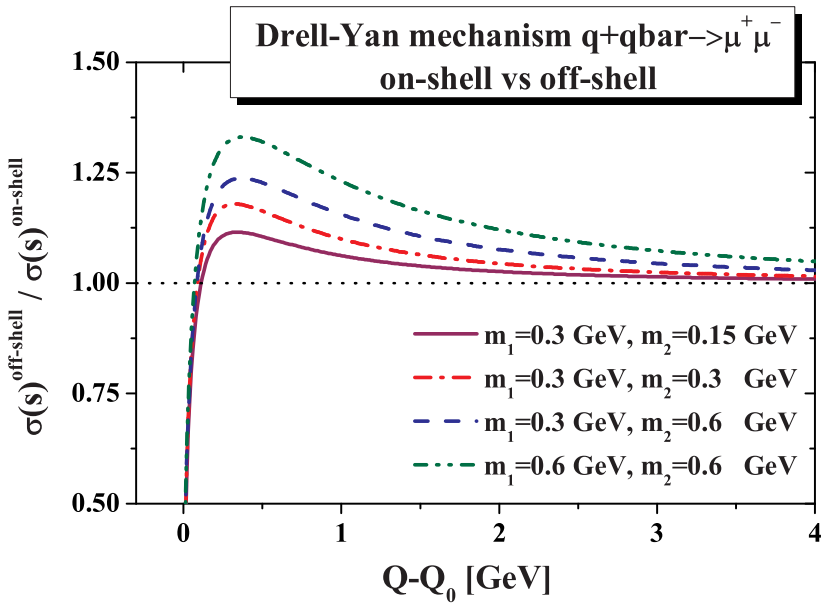

(b) Ratios of the cross sections

Figure 3. (color online) Dimuon production cross sections in the Drell-Yan channel ($q+\bar{q} \to \mu^+ + \mu^-$). **(a)** The cross section is presented versus the mass of the muon pair Q. The short dashes (black) line shows the on-shell, i.e. the standard perturbative result. The other lines show the off-shell cross section, in which the annihilating quark and antiquark have finite masses m_1 and m_2 with different values: $m_1 = 0.3$ GeV, $m_2 = 0.15$ GeV (solid magenta line), $m_1 = 0.3$ GeV, $m_2 = 0.3$ GeV (dash-dotted red line), $m_1 = 0.3$ GeV, $m_2 = 0.6$ GeV (dashed blue line), $m_1 = 0.6$ GeV, $m_2 = 0.6$ GeV (dash-dot-dot green line). **(b)** The ratio of the off-shell cross section to the on-shell result for the different values of quark and antiquark masses is plotted versus $Q - Q_0$, where Q_0 is the threshold value for the lepton pair mass. Line coding as in the figure (a).

off-shell cross section, in which the annihilating quark and antiquark have finite masses m_1 and m_2 with different values: $m_1 = 0.3$ GeV, $m_2 = 0.15$ GeV (solid magenta line), $m_1 = 0.3$ GeV, $m_2 = 0.3$ GeV (dash-dotted red line), $m_1 = 0.3$ GeV, $m_2 = 0.6$ GeV (dashed blue line), $m_1 = 0.6$ GeV, $m_2 = 0.6$ GeV (dash-dot-dot green line).

The importance of finite mass corrections in the Drell-Yan process is illustrated by the ratio of the integrated cross section $\sigma(Q)$ in Fig. 3 (b). The ratio of the off-shell cross section to the on-shell result for the different values of quark and antiquark masses is plotted versus $Q - Q_0$, where Q_0 is the threshold value for the lepton pair mass. The line coding is the same as in the previous figure. With increasing Q^2, the off-shell cross sections approach the leading twist – on-shell – result.

The observed deviations of the derived cross sections from the massless limit at low Q^2 should be seen in the dilepton rates from the sQGP created in heavy-ion collisions at relatively low dilepton masses. This question can be addressed by convoluting the off-shell cross section (14) with effective spectral functions $A(m_i)$ for quarks in plasma and with a model for the momentum distribution of quarks in plasma. We will return to this issue in Sections IV and V.

3.2. Off-shell gluon Bremsstrahlung $q\bar{q} \to gl^+l^-$

We start this section by stating the off-shell kinematics of the $q\bar{q} \to gl^+l^-$ process. The dilepton mass range is $4m_{lept}^2 < Q^2 < (\sqrt{s} - \mu)^2$, while the kinematical limits for the momentum transfer t are

$$t_{min}^{max} = -\frac{s}{2}(C_1 \pm C_2), \tag{15}$$

where

$$\begin{aligned} C_1 &= 1 - (\beta_1 + \beta_2 + \beta_3 + \beta_4) + (\beta_1 - \beta_2)(\beta_3 - \beta_4), \\ C_2 &= \sqrt{(1 - \beta_1 - \beta_2)^2 - 4\beta_1\beta_2} \\ &\quad \times \sqrt{(1 - \beta_3 - \beta_4)^2 - 4\beta_3\beta_4} \end{aligned} \tag{16}$$

with

$$\beta_1 = m_1^2/s,\ \beta_2 = m_2^2/s,\ \beta_3 = Q^2/s,\ \beta_4 = \mu^2/s. \tag{17}$$

Additionally, we note that there is a threshold in the CMS energy $\sqrt{s}$ for the $q + \bar{q}$ interaction:

$$s \geq \max\{(m_1 + m_2)^2, (\mu + Q)^2\}. \tag{18}$$

In contrast to the $q\bar{q} \to l^+l^-$ process, the off-shell cross section for the $q\bar{q}$ annihilation *with gluon Bremsstrahlung* in the final state has not been calculated before. Therefore, we will provide here a short description of its evaluation.

Starting from the formula for the unpolarized cross section

$$d\sigma = \frac{\Sigma|\bar{M_{i\to f}}|^2 \varepsilon_1\varepsilon_2 \Pi \frac{d^3p_f}{(2\pi)^3}}{\sqrt{(p_1p_2)^2 - m_1^2m_2^2}}\ (2\pi)^4\delta(p_1 + p_2 - \Sigma p_f), \tag{19}$$

where the incoming quark and antiquark momenta are p_1 and p_2 and their masses m_1 and m_2, respectively; p_f are the momenta of the outgoing particles, i.e. of the electron (muon) and positron (anti-muon) and gluon. We note that the dilepton production cross section can be easily obtained from the cross section for the production of virtual photons as

$$\frac{d\sigma(l^+l^-)}{dQ^2dt} = \frac{\alpha}{3\pi Q^2}\frac{d\sigma(\gamma^*)}{dt}FF(Q^2,Q_0^2) \tag{20}$$

with

$$FF(Q^2,Q_0^2) = \sqrt{1-\frac{Q_0^2}{Q^2}}\left(1+\frac{Q_0^2}{2Q^2}\right), \tag{21}$$

where $Q_0^2 = 4m_{lept}^2$ and m_{lept} is the lepton mass.

Furthermore, we define the momenta of the internal quark exchanged in the two relevant diagrams (see Fig. 1) as $p_3 \equiv p_1 - q$, $\bar{p}_3 \equiv p_1 - p_2 - p_3$ and its mass as m_3. The final gluon momentum is k and its mass is μ. Then the matrix element of the process $q + \bar{q} \to g + \gamma^*$ is

$$M = M_a + M_b, \tag{22}$$

where

$$M_a = -e_q e g_s T^l_{ij}\frac{\epsilon_\nu(q)\epsilon_{\sigma l}(k)}{p_3^2 - m_3^2}u_i(p_1,m_1)\left[\gamma^\nu(\hat{p}_3 + m_3)\gamma^\sigma\right]v_j(p_2,m_2) \tag{23}$$

and

$$M_b = -e_q e g_s T^l_{ij}\frac{\epsilon_{\sigma l}(k)\epsilon_\nu(q)}{\bar{p_3}^2 - m_3^2}u_i(p_1,m_1)\left[\gamma^\eta(\hat{\bar{p}}_3 + m_3)\gamma^\nu\right]v_j(p_2,m_2), \tag{24}$$

e is the electron charge while e_q is the quark fractional charge; T^l_{ij} is the generator of the SU(3) color group (that will yield the color factor in the cross section); $\epsilon_\nu(q)$ is the polarization vector for the virtual photon with momentum q; $\epsilon_{\sigma l}(k)$ is the polarization vector for the gluon of momentum k and color l; $u_i(p,m)$ is a Dirac spinor for the quark with momentum p, mass m and color i; and $v_i(p,m)$ is the spinor for the anti-quark.

The squared – and summed over spin polarizations as well as over color degrees of freedom – matrix element can be decomposed in the following summands:

$$\sum|M|^2 = \sum M_a^* M_a + \sum M_b^* M_b + \sum M_a^* M_b + \sum M_b^* M_b, \tag{25}$$

where the star denotes the complex conjugation.

The spinors for quark states with mass m_i contribute to the expression for the spin-averaged matrix element only in the combinations $\sum \bar{u}(p,m_i)u(p,m_i) = (\hat{p} + m_i)$ (cf [78]) and the correlation functions between the states with different masses does not enter $|M|^2$. Thus we find:

$$\sum M_a^* M_b \sim \frac{e_q^2 e^2 g_s^2 \mathrm{Tr}\{T^2\}}{(p_3^2 - m_3^2)(\bar{p_3}^2 - m_3^2)} \times \left[\mathrm{Tr}\left\{(\hat{p_2} - m_2)\gamma_\sigma(\hat{p_3} + m_3)\gamma_\nu(\hat{p_1} + m_1)\gamma^\sigma(\hat{\bar{p}_3} + m_3)\gamma^\nu\right\}\right.$$

$$
\begin{aligned}
&-\frac{1}{Q^2}\mathrm{Tr}\left\{(\hat{p_2}-m_2)\gamma_\sigma(\hat{p_3}+m_3)\hat{q}(\hat{p_1}+m_1)\gamma^\sigma(\hat{\bar{p_3}}+m_3)\hat{q}\right\}\\
&-\frac{A}{k^2}\mathrm{Tr}\left\{(\hat{p_2}-m_2)\hat{k}(\hat{p_3}+m_3)\gamma_\nu(\hat{p_1}+m_1)\hat{k}(\hat{\bar{p_3}}+m_3)\gamma^\nu\right\}\\
&+\frac{A}{k^2Q^2}\mathrm{Tr}\left\{(\hat{p_2}-m_2)\hat{k}(\hat{p_3}+m_3)\hat{q}(\hat{p_1}+m_1)\hat{k}(\hat{\bar{p_3}}+m_3)\hat{q}\right\}\Bigg], \quad (26)
\end{aligned}
$$

$$
\begin{aligned}
\sum|M_a|^2 =& -\frac{e_q^2e^2g_s^2\mathrm{Tr}\{T^2\}}{(p_3^2-m_3^2)^2}\\
&\times[\mathrm{Tr}\{\gamma_\sigma(\hat{p_3}+m_3)\gamma_\nu(\hat{p_1}+m_1)\gamma^\nu(\hat{p_3}+m_3)\gamma^\sigma(\hat{p_2}-m_2)\}\\
&-\frac{1}{Q^2}\mathrm{Tr}\{\gamma_\sigma(\hat{p_3}+m_3)\hat{q}(\hat{p_1}+m_1)\hat{q}(\hat{p_3}+m_3)\gamma^\sigma(\hat{p_2}-m_2)\}\\
&-\frac{A}{k^2}\mathrm{Tr}\left\{\hat{k}(\hat{p_3}+m_3)\gamma_\nu(\hat{p_1}+m_1)\gamma^\nu(\hat{p_3}+m_3)\hat{k}(\hat{p_2}-m_2)\right\}\\
&+\frac{A}{k^2Q^2}\mathrm{Tr}\left\{\hat{k}(\hat{p_3}+m_3)\hat{q}(\hat{p_1}+m_1)\hat{q}(\hat{p_3}+m_3)\hat{k}(\hat{p_2}-m_2)\right\}\Bigg]. \quad (27)
\end{aligned}
$$

Note that we can readily obtain $\sum M_b^* M_a$ from $\sum M_a^* M_b$ and $\sum |M_b|^2$ from $\sum |M_a|^2$ by the transformation $\{p_3 \to \bar{p_3}, p_1 \to p_2, p_2 \to p_1, m_1 \to -m_2, m_2 \to -m_1\}$. In equations (26) and (27), A sets the gauge and we will discuss the dependance on A later on. We used the feynpar.m [79] package of the Mathematica program [80] to evaluate the traces of the products of the gamma matrices. The resulting cross section is (here shown for $A = 1$):

$$
\begin{aligned}
&\left(\frac{d\hat{\sigma}(q\,\bar{q}\to g\,l^+l^-)}{dQ^2dt}\right)^{gBr}_{offshell} =\\
&\quad -\frac{\alpha^2\,\alpha_S\,{e_q}^2\,\Theta\left(-Q^2+s+t-\mu^2\right)\delta(s+t+u-m_1^2-m_2^2-Q^2-\mu^2)}{27\,Q^4\sqrt{-2\,({m_1}^2\,{m_2}^2)+\left({m_1}^2+{m_2}^2-s\right)^2}\,s\,\left({m_3}^2-t\right)\,\left({m_3}^2-u\right)\,\mu^2}\\
&\times\Big[{m_3}^6\,\left(s\,t\,(s+t)+(s+2\,t)^2\,u+(s+4\,t)\,u^2-Q^4\,(t+u)+Q^2\,\left(t^2+u^2\right)\right)\\
&+t\,u\,\left(-2\,Q^6\,(t+u)+2\,t\,u\,(2\,s\,(s+t)+(2\,s+t)\,u)+4\,Q^4\,\left(t^2+u^2+s\,(t+u)\right)\right.\\
&\left.-Q^2\,\left(2\,s^2\,(t+u)+4\,s\,\left(t^2+u^2\right)+(t+u)\,\left(2\,t^2-3\,t\,u+2\,u^2\right)\right)\right)+{m_3}^2\,\left(2\,Q^6\,(t+u)^2\right.\\
&-Q^4\,(t+u)\,\left(4\,t\,(s+t)+(4\,s+t)\,u+4\,u^2\right)+2\,Q^2\,\left(t^4+t^3\,u-t^2\,u^2+t\,u^3+u^4\right.\\
&+s^2\,(t+u)^2+2\,s\,(t+u)\,\left(t^2+u^2\right)\Big)+t\,u\,\left(-3\,s^2\,(t+u)-2\,s\,\left(t^2+3\,t\,u+u^2\right)\right.\\
&\left.\left.+2\,\left(t^3+u^3\right)\right)\right)-{m_3}^4\,\left(-\left(s^2\,(t-u)^2\right)+2\,Q^6\,(t+u)-2\,s\,(t+u)\,\left(t^2-3\,t\,u+u^2\right)\right.\\
&+t\,u\,\left(3\,t^2+8\,t\,u+3\,u^2\right)-Q^4\,\left(5\,t^2+2\,t\,u+5\,u^2+4\,s\,(t+u)\right)+Q^2\,\left(2\,s^2\,(t+u)\right.\\
&\left.\left.+4\,s\,\left(t^2+u^2\right)+3\,\left(t^3+u^3\right)\right)\right)-m_1\,m_3\,\left(t\,u\,\left(2\,Q^4\,(t+u)+s^2\,(t+u)\right.\right.\\
&\left.-Q^2\,\left(t^2+12\,t\,u+u^2+3\,s\,(t+u)\right)\right)+{m_3}^2\,(t+u)\,\left(-2\,Q^4\,(t+u)-s^2\,(t+u)\right.\\
&\left.+Q^2\,\left(t^2+12\,t\,u+u^2+3\,s\,(t+u)\right)\right)+{m_3}^4\,\left(2\,Q^4\,(t+u)+s^2\,(t+u)-Q^2\,(3\,s\,(t+u)\right.\\
&\left.\left.+7\,\left(t^2+u^2\right)\right)\right)\Big)+\Big(-\left({m_3}^6\,\left(6\,Q^4+2\,s^2+t^2+u^2-5\,Q^2\,(t+u)+4\,s\,(t+u)\right)\right)
\end{aligned}
$$

$$
\begin{aligned}
&+t\,u\,\left(-8\,Q^6+t\,u\,\left(2\,s+t+u\right)+Q^4\,\left(-4\,s+7\,\left(t+u\right)\right)+Q^2\,\left(4\,s^2+2\,{\left(t-u\right)}^2\right.\right.\\
&\left.+5\,s\,\left(t+u\right)\right))+{m_3}^4\,\left(-8\,Q^6+2\,t\,{\left(s+t\right)}^2+\left(2\,s^2+10\,s\,t+t^2\right)\,u+\left(4\,s+t\right)\,u^2+2\,u^3\right.\\
&\left.+Q^4\,\left(-4\,s+13\,\left(t+u\right)\right)+Q^2\,\left(4\,s^2+5\,s\,\left(t+u\right)-2\,\left(t^2+8\,t\,u+u^2\right)\right)\right)\\
&+{m_3}^2\,\left(8\,Q^6\,\left(t+u\right)+Q^4\,\left(-7\,t^2-20\,t\,u-7\,u^2+4\,s\,\left(t+u\right)\right)-t\,u\,\left(2\,s^2+6\,s\,\left(t+u\right)\right.\right.\\
&\left.\left.+3\,\left(t^2+u^2\right)\right)-Q^2\,\left(4\,s^2\,\left(t+u\right)+\left(t+u\right)\,\left(4\,t^2-13\,t\,u+4\,u^2\right)+s\,\left(7\,t^2+6\,t\,u+7\,u^2\right)\right)\right)\\
&+m_1\,m_3\,\left(-\left({m_3}^4\,\left(10\,Q^4-2\,s^2+t^2+u^2-s\,\left(t+u\right)+2\,Q^2\,\left(2\,s+t+u\right)\right)\right)-t\,u\,\left(10\,Q^4\right.\right.\\
&\left.-2\,s^2+t^2+u^2-s\,\left(t+u\right)+2\,Q^2\,\left(2\,s+t+u\right)\right)+{m_3}^2\,\left(10\,Q^4\,\left(t+u\right)+\left(t+u\right)\,\left(-2\,s^2\right.\right.\\
&\left.\left.\left.\left.+t^2+u^2-s\,\left(t+u\right)\right)+4\,Q^2\,\left(-t^2+4\,t\,u-u^2+s\,\left(t+u\right)\right)\right)\right)\right)\,\mu^2\\
&+\left({m_3}^2-t\right)\,\left({m_3}^2-u\right)\,\left(4\,m_1\,m_3\,Q^2-12\,{m_3}^2\,Q^2-10\,Q^4-4\,m_1\,m_3\,s+4\,{m_3}^2\,s-6\,Q^2\,s\right.\\
&\left.+4\,{m_3}^2\,t+3\,Q^2\,t-s\,t-t^2+4\,{m_3}^2\,u+3\,Q^2\,u-s\,u-4\,t\,u-u^2\right)\,\mu^4\\
&+\left({m_3}^2-t\right)\,\left({m_3}^2-u\right)\,\left(2\,\left(m_1-m_3\right)\,m_3-2\,Q^2+t+u\right)\,\mu^6+2\,{m_2}^6\,\left({m_3}^2-t\right)\,\left({m_3}^2\right.\\
&\left.-u\right)\,\left(2\,Q^2-s+\mu^2\right)+{m_2}^4\,\left({m_3}^2-t\right)\,\left({m_3}^2-u\right)\,\left(2\,m_1\,m_3\,Q^2+2\,{m_3}^2\,Q^2+4\,Q^4-6\,Q^2\,s\right.\\
&\left.+2\,s^2-5\,Q^2\,t+2\,s\,t-5\,Q^2\,u+2\,s\,u-2\,\left(m_3\,\left(m_1+m_3\right)+t+u\right)\,\mu^2-4\,\mu^4\right)-2\,{m_2}^5\,\left({m_3}^2\right.\\
&\left.-t\right)\,\left({m_3}^2-u\right)\,\left(m_1\,s+m_3\,\left(3\,Q^2-2\,s+3\,\mu^2\right)\right)\\
&-2\,{m_2}^3\,\left({m_3}^2-t\right)\,\left({m_3}^2-u\right)\,\left(-\left(m_1\,s\,\left(-Q^2+s+t+u-\mu^2\right)\right)+m_3\,\left(Q^4\right.\right.\\
&\left.\left.-3\,Q^2\,\left(s+t+u\right)+2\,s\,\left(s+t+u\right)-3\,\left(s+t+u\right)\,\mu^2+\mu^4\right)\right)-{m_2}^2\,\left({m_3}^2-t\right)\,\left({m_3}^2\right.\\
&\left.-u\right)\,\left(2\,s\,t\,u+\left(4\,s^2-2\,t\,u+3\,s\,\left(t+u\right)\right)\,\mu^2-5\,\left(2\,s+t+u\right)\,\mu^4+6\,\mu^6+5\,Q^4\,\left(t+u-2\,\mu^2\right)\right.\\
&\left.-2\,{m_3}^2\,\left(Q-\mu\right)\,\left(Q+\mu\right)\,\left(2\,Q^2-2\,s-t-u+2\,\mu^2\right)-Q^2\,\left(5\,t^2-2\,t\,u+5\,u^2+5\,s\,\left(t+u\right)\right.\right.\\
&\left.\left.+2\,s\,\mu^2-8\,\left(t+u\right)\,\mu^2+2\,\mu^4\right)+2\,m_1\,m_3\,\left(s^2-\left(3\,s+t+u\right)\,\mu^2+2\,\mu^4\right.\right.\\
&\left.\left.\left.+Q^2\,\left(-s+t+u-4\,\mu^2\right)\right)\right)-m_2\,\left(m_1\,\left(-2\,{m_3}^6\,\left(Q^4-2\,Q^2\,\left(s-5\,\mu^2\right)\right.\right.\right.\\
&\left.\left.\left.+{\left(s-\mu^2\right)}^2\right)+t\,u\,\left(2\,s\,t\,u+\left({\left(t-u\right)}^2+s\,\left(t+u\right)\right)\,\mu^2-\left(t+u\right)\,\mu^4\right.\right.\right.\\
&\left.\left.\left.-Q^4\,\left(t+u-4\,\mu^2\right)+Q^2\,\left({\left(t-u\right)}^2+s\,\left(t+u\right)-26\,\left(t+u\right)\,\mu^2+4\,\mu^4\right)\right)\right.\\
&\left.+{m_3}^4\,\left(2\,s\,t\,u+2\,s^2\,\left(t+u\right)+{\left(t-u\right)}^2\,\mu^2-3\,s\,\left(t+u\right)\,\mu^2+\left(t+u\right)\,\mu^4\right.\right.\\
&\left.\left.+Q^4\,\left(t+u+4\,\mu^2\right)+Q^2\,\left({\left(t-u\right)}^2-3\,s\,\left(t+u\right)-6\,\left(t+u\right)\,\mu^2+4\,\mu^4\right)\right)\right.\\
&\left.+{m_3}^2\,\left(-2\,s\,t\,u\,\left(s+t+u\right)+\left(t^2+u^2\right)\,\mu^4-{\left(t-u\right)}^2\,\left(s+t+u\right)\,\mu^2\right.\right.\\
&\left.\left.+Q^4\,\left(t^2+u^2-4\,\left(t+u\right)\,\mu^2\right)+Q^2\,\left(-\left({\left(t-u\right)}^2\,\left(s+t+u\right)\right)-2\,\left(5\,t^2+5\,u^2\right.\right.\right.\right.\\
&\left.\left.\left.\left.-52\,t\,u\right)\,\mu^2-4\,\left(t+u\right)\,\mu^4\right)\right)\right)+m_3\,\left(t\,u\,\left(-4\,Q^6-4\,s\,t\,u+Q^4\,\left(8\,s+t+u\right)\right.\right.\\
&\left.\left.+Q^2\,\left(-4\,s^2+t^2+4\,t\,u+u^2-s\,\left(t+u\right)\right)\right)-\left(12\,t^2\,{\left(s+t\right)}^2+t\,\left(-4\,Q^4+4\,s^2\right.\right.\right.\\
&\left.\left.\left.+19\,s\,t+17\,t^2+Q^2\,\left(-12\,s+8\,t\right)\right)\,u+\left(12\,s^2+8\,Q^2\,t+19\,s\,t-4\,t^2\right)\,u^2\right.\right.\\
&\left.\left.+\left(24\,s+17\,t\right)\,u^3+12\,u^4\right)\,\mu^2+t\,u\,\left(4\,Q^2+8\,s+t+u\right)\,\mu^4-4\,t\,u\,\mu^6
\end{aligned}
$$

$$+{m_3}^2\,\Big(-\Big((t+u)\,\Big(-4\,Q^6-4\,s\,t\,u+Q^4\,(8\,s+t+u)+Q^2\,\Big(-4\,s^2+t^2 +4\,t\,u+u^2-s\,(t+u)\Big)\Big)\Big)+\Big(-4\,Q^4\,(t+u)+28\,s^2\,(t+u)+(t+u)\,\Big(23\,t^2 +8\,t\,u+23\,u^2\Big)+s\,\Big(49\,t^2+74\,t\,u+49\,u^2\Big)+4\,Q^2\,(t+u)\,(-3\,s+2\,(t+u))\Big)\,\mu^2 -(t+u)\,\Big(4\,Q^2+8\,s+t+u\Big)\,\mu^4+4\,(t+u)\,\mu^6\Big)+{m_3}^4\,\Big(-4\,Q^6-4\,s\,t\,u -\Big(28\,s^2+11\,t^2+32\,t\,u+11\,u^2+43\,s\,(t+u)\Big)\,\mu^2+(8\,s+t+u)\,\mu^4 -4\,\mu^6+Q^4\,\Big(8\,s+t+u+4\,\mu^2\Big)+Q^2\,\Big(-4\,s^2+t^2+4\,t\,u+u^2-8\,(t+u)\,\mu^2 +4\,\mu^4-s\,\Big(t+u-12\,\mu^2\Big)\Big)\Big)\Big)\Big]\qquad(28)$$

One can check that the expression (28) for $m_i \to 0$ approaches the leading twist pQCD result, where $\mu_{cut} = \mu$. We illustrate this in Fig. 4 where the off-shell cross sections for the quark annihilation with gluon bremsstrahlung at various values of quark and gluon off-shellnesses (masses) are compared to the on-shell (pQCD) result. The dashed black line shows the on-shell cross section for $\mu_{cut} = 0.206$ GeV, the red solid line presents the off-shell cross section for the gluon mass fixed to $\mu = 0.8$ GeV and on-shell quark and anti-quark ($m_1 = m_2 = m_3 = 0$). The blue dash-dotted line gives the off-shell result for $\mu = 0.8$ GeV, $m_1 = m_2 = m_3 = m_q = 0.6$ GeV. One readily notices the shift of the maximum pair mass to a lower value (in order to produce a massive gluon in the final state). For the rest of the Q values, the effect of the quark and gluon off-shellness reaches at most 50% as seen in the ratios of the cross sections, plotted in Fig. 4 (b).

Next we compare the double differential off-shell and on-shell cross sections. The results for the transverse momentum distributions of the dileptons are presented in Fig. 5. The solid black line shows the differential on-shell cross section with $\mu_{cut} = 0.206$ GeV, the blue dashed line presents the off-shell cross section for the gluon mass fixed to $\mu = 0.8$ GeV and on-shell quark and anti-quark ($m_1 = m_2 = m_3 = 0$). The red dash-dotted line gives the off-shell result for $\mu = 0.8$ GeV, $m_1 = m_2 = m_3 = m_q = 0.6$ GeV. Again, we find the largest effect at the edge of the phase space, at the minimal q_T.

3.3. Off-shell gluon Compton scattering $gq \to ql^+l^-$

Kinematic limits for s, t, Q^2 in the off-shell GCS process are analogous to the $q + \bar{q}$ case. In the off-shell case, the dilepton mass range is $4m_{lept}^2 < Q^2 < (\sqrt{s} - m_2)^2$, while the kinematical limits on the momentum transfer t are given by the Eqs. (15)-(16) with

$$\beta_1 = m_1^2/s,\ \beta_2 = \mu^2/s,\ \beta_3 = Q^2/s,\ \beta_4 = m_2^2/s, \qquad (29)$$

while

$$s \geq \max\{(m_1+\mu)^2, (m_2+Q)^2\},$$

where m_1 (m_2) is the mass of the incoming (outgoing) quark and μ is the mass of the gluon.

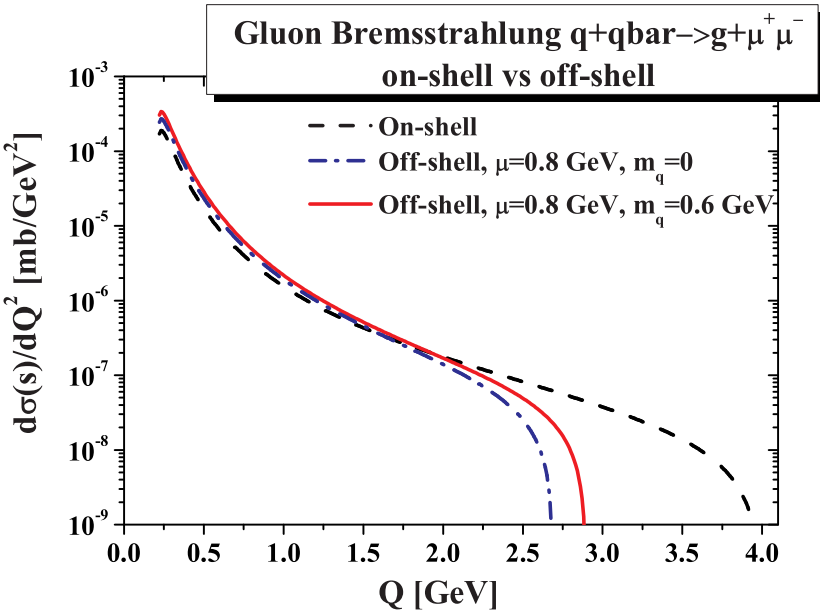

(a) Cross sections

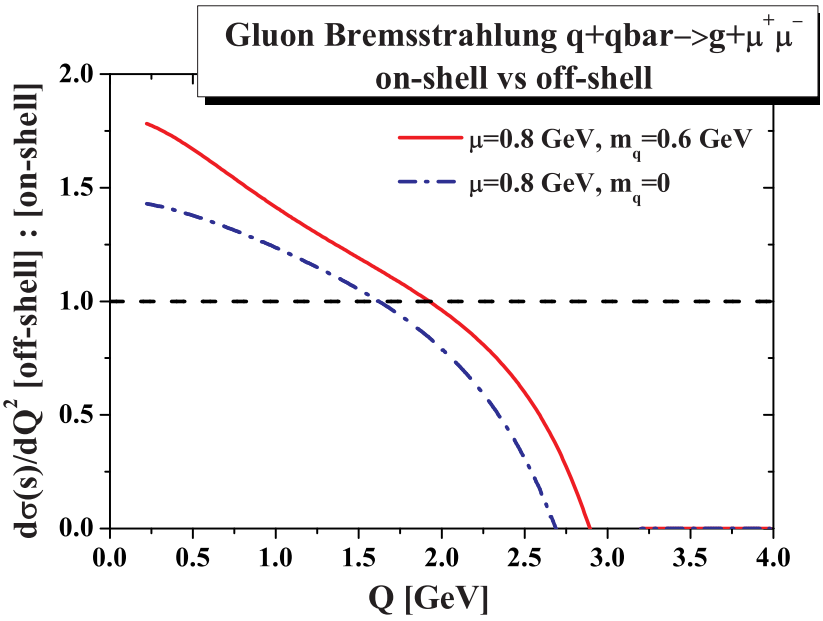

(b) Ratios of the cross sections

Figure 4. (color online) Comparison of off-shell and on-shell gluon Bremsstrahlung $q + \bar{q} \to g + \mu^+\mu^-$ cross sections at $\sqrt{s} = 4$ GeV. **(a)** The dashed black line shows the on-shell cross section with $\mu_{cut} = 0.206$ GeV, the blue dash-dotted line presents the off-shell cross section for the gluon mass fixed to $\mu = 0.8$ GeV and on-shell quark and anti-quark ($m_1 = m_2 = m_3 = 0$). The red solid line gives the off-shell result for $\mu = 0.8$ GeV, $m_1 = m_2 = m_3 = m_q = 0.6$ GeV. **(b)** The ratio of off-shell to on-shell cross sections using the same line coding is as in (a).

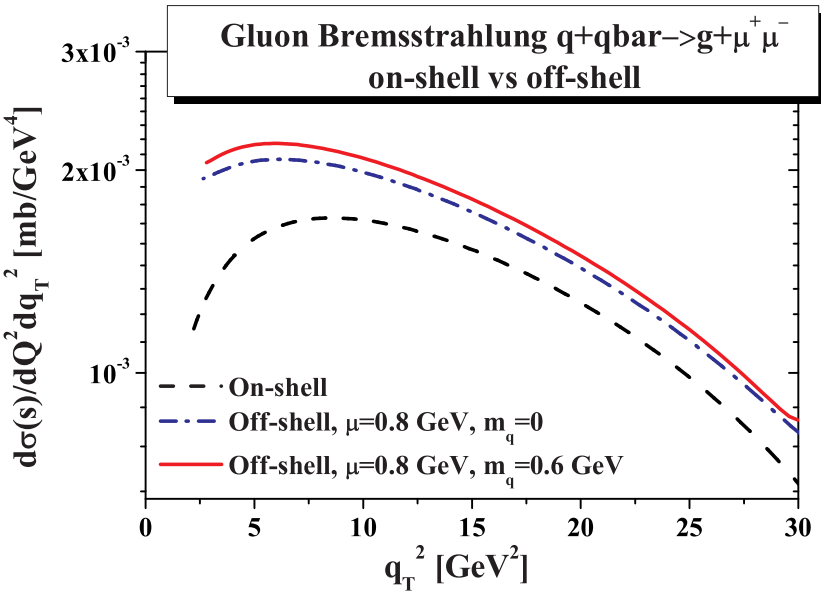

(a) Cross sections

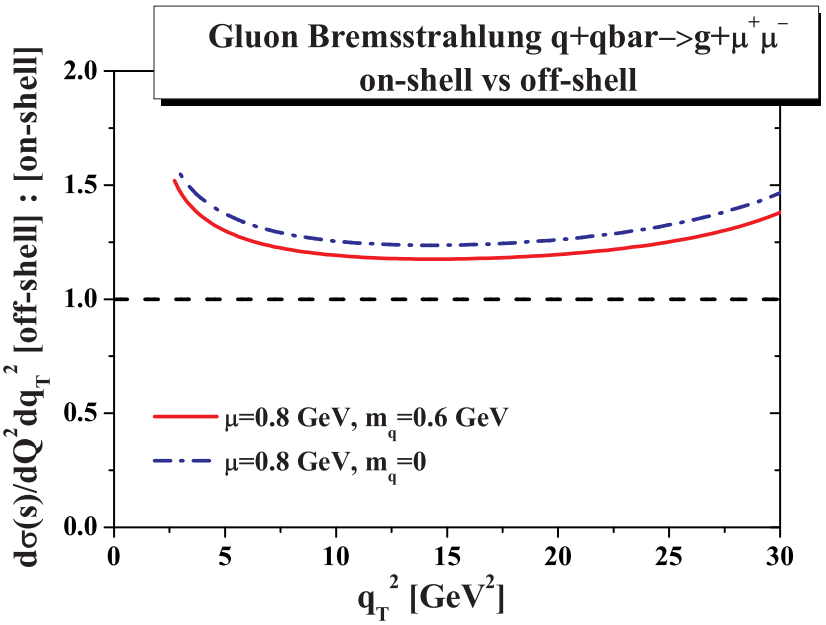

(b) Ratios of the cross sections

Figure 5. (color online) Comparison of the transverse momentum distributions of muon pairs produced in the gluon Bremsstrahlung $q + \bar{q} \to g + \mu^+\mu^-$ channel in the off-shell and on-shell cases. **(a)** The dashed black line shows the differential on-shell cross section with $\mu_{cut} = 0.206$ GeV, the blue dash-dotted line presents the off-shell cross section for the gluon mass fixed to $\mu = 0.8$ GeV and on-shell quark and anti-quark ($m_1 = m_2 = m_3 = 0$). The red solid line gives the off-shell result for $\mu = 0.8$ GeV, $m_1 = m_2 = m_3 = m_q = 0.6$ GeV. **(b)** The ratio of off-shell to on-shell cross sections using the same line coding.

The cross section for gluon Compton scattering can be calculated analogously to the calculation of the gluon Bremststrahlung cross section (28) above. On the other hand, the cross sections for $g + q \to q + l^+ + l^-$ and $g + \bar{q} \to \bar{q} + l^+ + l^-$ are readily obtained from (28) by the crossing transformation.

3.4. Virtual gluon decay $g \to q\bar{q}l^+l^-$ and virtual quark decay $q \to gql^+l^-$

Although the process of real gluon decay $g \to q + \bar{q} + l^+l^-$ is forbidden kinematically for perturbative particles, it has a finite region of phase space, if the gluon is off-shell due to its broad with and finite pole mass. Analogously, the virtual quark decay is also possible in the off-shell case. We present the Feynman diagrams for the corresponding processes in Fig. 2. The off-shell cross sections for these processes can straightforwardly be obtained from (28) by the crossing relation. For example, the cross section for $q \to gql^+l^-$ is obtained from $q\bar{\to}gl^+l^-$ by changing $p_2 \to -p_2$.

Note that, in order to obtain the dilepton rates, the elementary cross sections have to be consequently convoluted with the effective spectral functions for quarks and gluons. The magnitude and shape of the contributions of the virtual decays to the dilepton rates is very sensitive to the final choice of the spectral function. In the DQPM the contribution from gluon decay is higher than that from virtual quark decay, since the gluonic quasi-particles are more massive and broader than the quarks [31], and thus the kinematically allowed region is larger for the virtual gluon than for the virtual quark decay.

On the other hand, within the DQPM parametrizations for the partonic spectral functions, both processes presented by the diagrams in Fig. 2 generate little dilepton yield anywhere except for extremely low masses: $Q \approx 2m_{muon}$. Therefore, we refrain from plotting here the contributions explicitly and also do not consider them in the next section dedicated to a comparison of the yields from different mechanisms.

4. Contributions of different processes to the dilepton rates from the QGP

In the following we are going to model the contributions of the different processes to the dilepton yield of the strongly coupled quark-gluon plasma. Using the factorization formula (12), we calculate the dilepton emission from the QGP by the convolution of the elementary sub-process cross sections with the distribution of the quarks and gluons with different momenta and virtualities. The elementary cross sections $\hat{\sigma}_{abc}(\hat{s}, m^{i1}, m^{i2}, \mu^f)$ for the different processes have been presented in the previous Section.

In Eq. (12) we integrate over the motion of partons, but also over their virtualities by employing phenomenological structure functions F_{ab} that depend on the invariant energy $\hat{s}$ of the partonic sub-process as well as on the virtualities of the incoming partons and the spectral function $\mathrm{A}(\mu^f)$ for the parton in the final state. Here, in principle, should be a two particle correlator, but we work in the 2PI approximation so

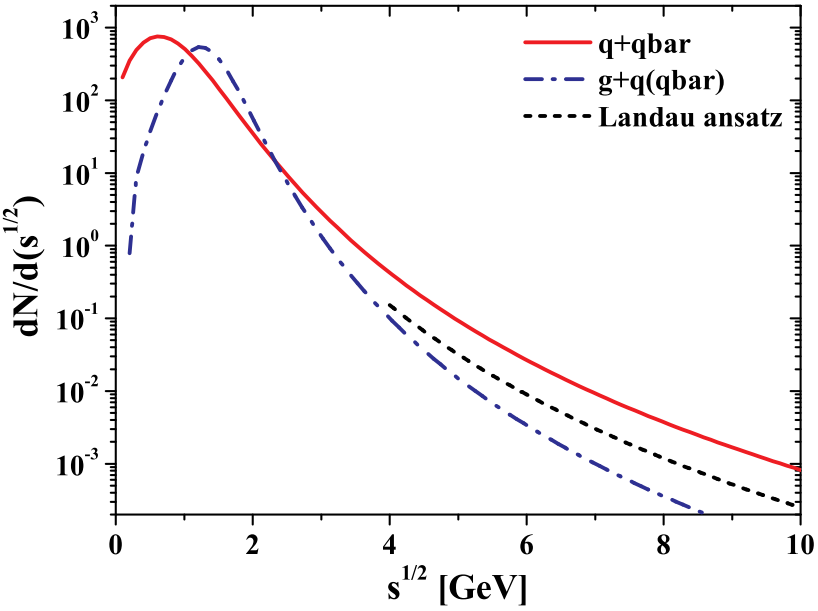

Figure 6. (color online) The number of $q+\bar{q}$ (red solid line) and $g+q(g+\bar{q})$ (blue dashed line) collisions versus $\sqrt{s}$. The black dashed line shows for comparison the prediction in the Landau model for the heavy-ion collision – the power law fall is $\sim(\sqrt{s})^{-7}$.

that the parton in the sQGP can be characterized by a single-particle distribution. We, therefore, we assume that the plasma structure function can be approximated by

$$F_{ab}(\hat{s}, m_1, m_2) = A_a(m_1)A_b(m_2)\frac{dN_{ab}}{ds}. \tag{30}$$

In this context, the quantity $dN_{q\bar{q}}/ds$ has the meaning of the number of $q+\bar{q}$ collisions in the plasma as a function of the invariant energy of these collisions $\sqrt{s}$. Analogously, dN_{gq}/ds denotes the number of $g+q$ collisions.

In order to address the relative importance of the different mechanisms for the dilepton production in the sQGP, we need a quantitative model for the number of $q+\bar{q}$ and $g+q$ $(g+\bar{q})$ collisions as functions of $\sqrt{s}$ of these collisions. In earlier works [4, 6, 8, 43, 83], thermal distributions of massless quarks and gluons have been used in order to estimate the number of parton collisions. However, we choose to use here more realistic dN/ds distributions, inspired by simulations in the parton transport model PHSD [84] and presented in Fig. 6 by a red solid line for $q+\bar{q}$ and by a blue dash-dotted line for $g+q$. We note that at high $\sqrt{s}$ the distributions approach the Landau ansatz (const $\cdot\, T^{-7}$), which is shown in Fig. 6 by the black dotted line. Indeed, in the Landau model for heavy-ion collisions, the parametrizations fall off with temperature according to the power low $\phi(T) \sim T^{-7}$ [4], while the energy of parton collisions is on average proportional to the temperature $\sqrt{s} \sim T$. The maximum of $dN(q+\bar{q})/d\sqrt{s}$ is at $\sqrt{s}\approx 0.5$ GeV and the maximum of $dN(g+q)/d\sqrt{s}$ is at a higher value of $\sqrt{s}\approx 1.2$ GeV, reflecting the fact that the threshold $\sqrt{s_0} = m_a + m_b$ is higher for gq than for qq

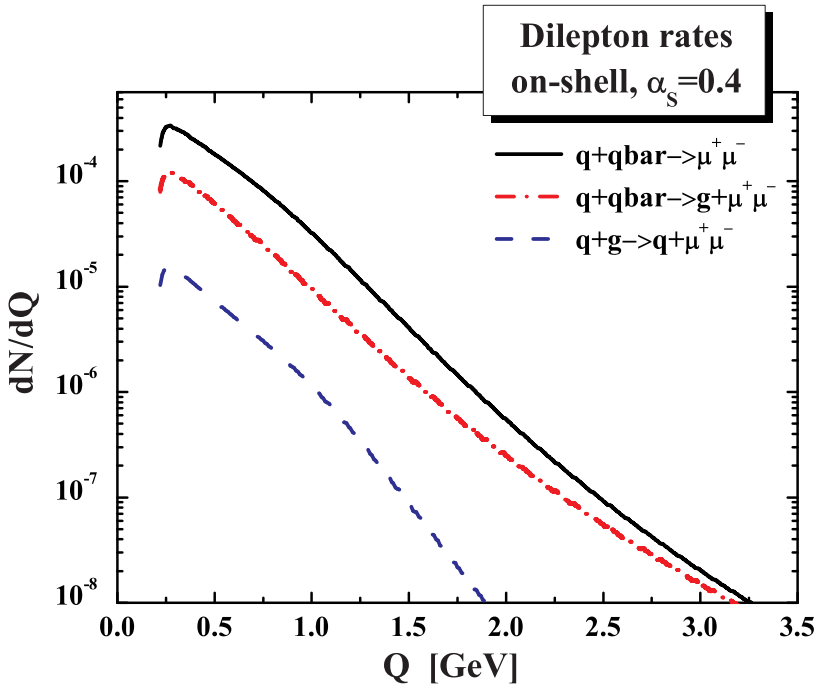

Figure 7. (color online) Dimuon rates dN/dQ from QGP calculated using the cross sections in the on-shell approximation, $\alpha_S = 0.4$. Black solid line shows the contribution of the Drell-Yan channel ($q + \bar{q} \to \mu^+\mu^-$), red dash-dotted line represents the contribution of the channel $q + \bar{q} \to g + \mu^-\mu^+$, blue dashed line shows the contribution of the channel $q + g \to q + \mu^+\mu^-$.

collisions. Indeed, the gluonic quasi-particles are expected to be more massive than the quark ones [31]. The functional form for $dN/d\sqrt{s}$ is taken as

$$\frac{dN_{ab}}{d\sqrt{s}} = K_{ab}\, s^{1/4} \left[(\sqrt{s} - P_{ab})^2 + W_{ab}\right]^{-3.5} \tag{31}$$

with ($P_{qq} = 0.5$, $W_{qq} = 1.2$) for $q\bar{q}$ collisions and ($P_{gq} = 1.2$, $W_{gq} = 0.6$) for gq collisions.

In Fig. 7 we plot the dilepton spectrum calculated using Eq. (12) and the cross sections given in Section 3 assuming $\alpha_S = 0.4$‡. One observes that after the convolution with the distribution of possible $\sqrt{s}$ for the $q + \bar{q}$ annihilation in sQGP, the yield of lepton pairs produced in the Bremsstrahlung process is below the leading order Born contribution. Thus, the Born rate is higher in magnitude than that of the gluon Bremsstrahlung process despite the fact that the former one contributes only to lepton pairs with a mass equal to the $\sqrt{s}$.

On the other hand, one notices from Fig. 7 that the GCS mechanism is sub-leading, unless the gluonic content of the plasma is orders of magnitude above the quark content, which is achieved neither at SPS nor at RHIC energies. A very high gluon content might

‡ The absolute magnitudes of the dilepton rates presented in Figs.10,14,15 and 16 should not be directly compared to experimental data. The analysis of the relative yields serves as an illustration of an application of the off-shell cross sections.

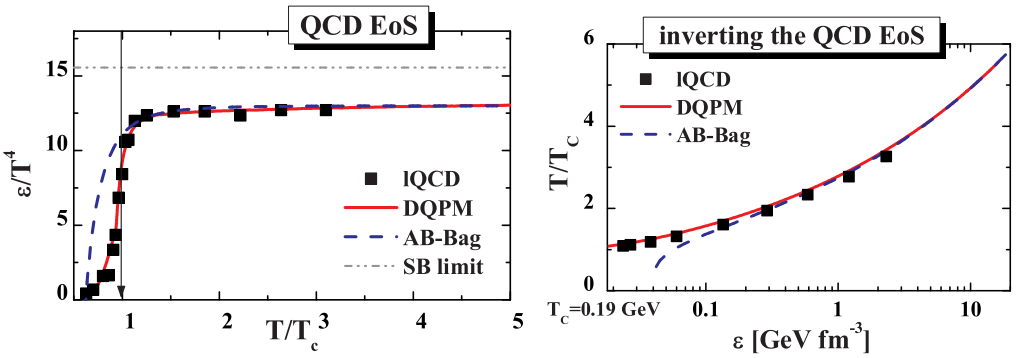

Figure 8. (color online) **L.h.s.** QCD energy density versus temperature from lattice QCD (square symbols) [81], the DQPM approach (red solid line) [31] and the 'A-Bag' model (blue dashed line) [82]. The grey dash-dotted line shows the Stefan-Boltzmann limit. The arrow indicates the critical temperature. **R.h.s.** Temperature as a function of the energy density from lattice QCD (square symbols) [81], the DQPM approach (red solid line) [31] and the 'A-Bag' model (blue dashed line) [82].

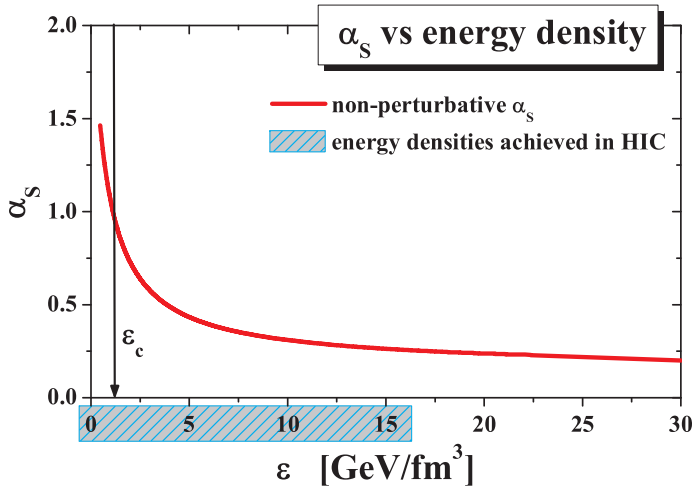

Figure 9. (color online) Non-perturbative running coupling as a function of the local energy density ε. The shadowed area indicates the energy densities reached in heavy ion collisions at SPS and RHIC. The arrow shows the critical energy-density.

be found at LHC; in this case the GCS process would give a considerable contribution to the dilepton yield.

Let us remind that the running coupling α_S depends on the local energy density ε. The DQPM [54] provides a good parametrization of the QCD running coupling as a function of temperature in the non-perturbative regime for temperatures close to T_c (cf. Fig. 1 in Ref. [54]). Note that close to T_c the full coupling calculated on the lattice increases with the decreasing temperature much faster than the pQCD prediction.

The energy density as a function of temperature has also been calculated on the lattice [81] (cf. Fig. 8). A rather simple parametrization for the QCD energy density – the "A-Bag model" – is proposed in Ref. [82] and provides a good fit of the SU(3) lattice

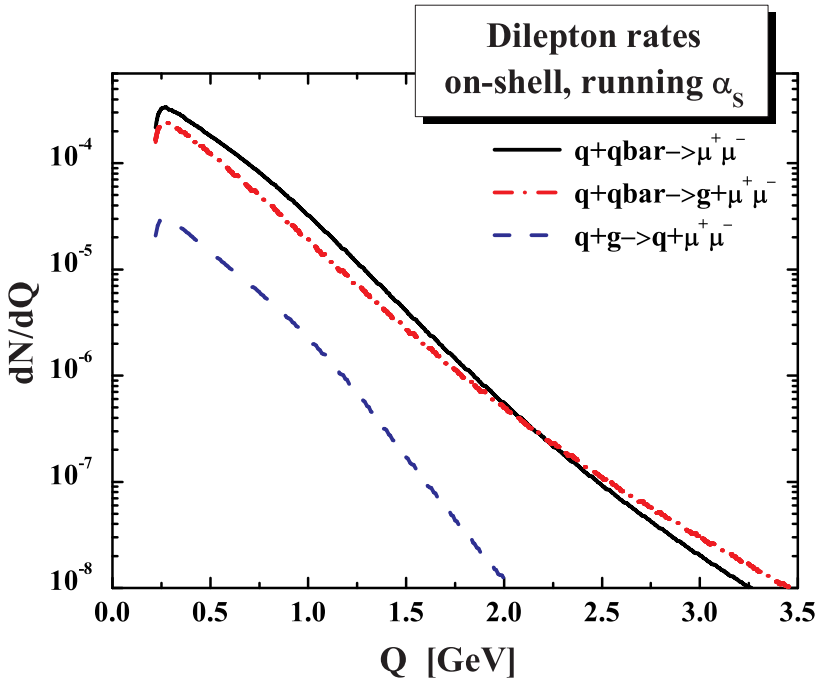

Figure 10. (color online) Dimuon rates dN/dQ from the QGP calculated using the cross sections in the on-shell approximation, $\alpha_S = 0.8$. Black solid line shows the contribution of the Drell-Yan channel ($q + \bar{q} \rightarrow \mu^+\mu^-$), the red dash-dotted line represents the contribution of the channel $q + \bar{q} \rightarrow g + \mu^-\mu^+$, the blue dashed line shows the contribution of the channel $q + g \rightarrow q + \mu^+\mu^-$.

data above T_c; we extend this model to 3-flavors and also compare to lattice data from Ref. [81] in Fig 8. On the other hand, the DQPM model describes the QCD energy density at temperatures even as low as $T \sim T_c$ [31]. In Fig 8 we invert the relation and present the temperature as a function of the energy density.

Using this relation, we obtain the running coupling as a function of the energy density ε instead of T/T_c; we present α_S vs. ε in Fig. 9. On the other hand, simulations in transport theory [85] have shown that the local energy densities achieved in the course of heavy-ion collisions at SPS and RHIC energies reach at most 20 GeV/fm^3; this region is high-lighted in Fig. 9 by a shadowed area. One observes that α_S at the energy densities of interest is on average 0.8. Using this value for α_S, we compare the rates in Fig. 10. In this case, the contribution of the $O(\alpha_S)$ diagrams (gluon-Compton scattering $qg \rightarrow q\gamma^*$ and gluon Bremsstrahlung $q\bar{q} \rightarrow g\gamma^*$) is no more subleading to the Born $q + \bar{q}$ annihilation mechanism!

Next, we plot the dilepton rates – within our approximation for the number of parton collisions in the plasma – for the case of *massive* quarks and gluons in Fig. 11. The rates are calculated by convoluting the off-shell cross sections obtained in the previous Section with our model $dN/d\sqrt{s}$. Quarks and gluons are massive quasi-particles, quark masses being set to $m_q = 0.3$ GeV and gluon mass $\mu = 0.8$ GeV. The black solid line shows the contribution of the channel $q+\bar{q} \rightarrow \mu^+\mu^-$, the red dash-dotted line represents

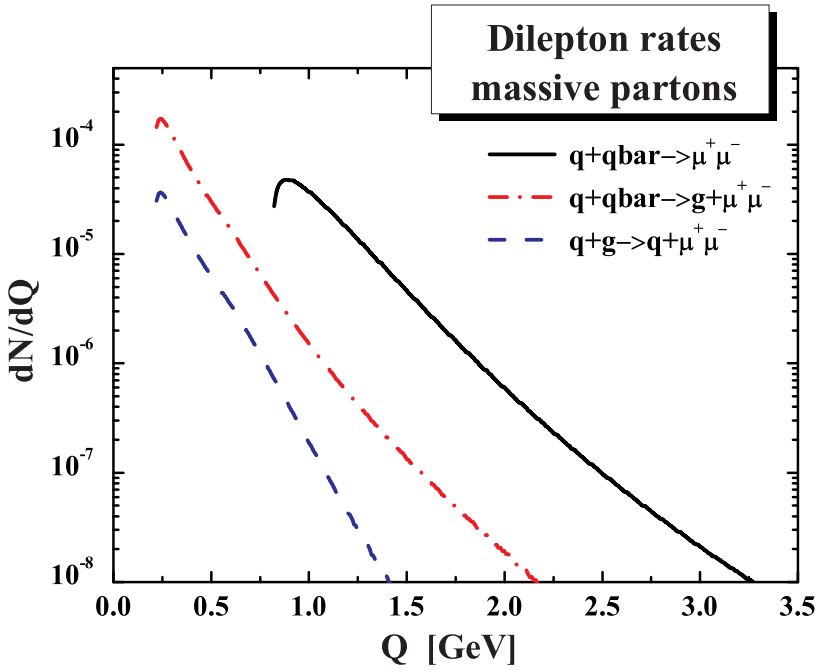

Figure 11. (color online) Dimuon rates from the QGP dN/dy beyond the on-shell approximation, $\alpha_S = 0.8$. dN/dQ calculated using the cross sections for quarks and gluons as massive quasi-particles, quark mass parameter being set to $m_q = 0.3$ GeV and gluon mass parameter to $\mu = 0.8$ GeV. The black solid line shows the contribution of the Drell-Yan channel ($q + \bar{q} \to \mu^+\mu^-$), the red dash-dotted line represents the contribution of the channel $q+\bar{q} \to g+\mu^-\mu^+$, blue dashed line shows the contribution of the channel $q + g \to q + \mu^+\mu^-$.

the contribution of the channel $q+\bar{q} \to g+\mu^-\mu^+$, blue dashed line shows the contribution of the channel $q+g \to q+\mu^+\mu^-$. The rates in the three channels are modified compared to the massless case (cf. Fig. 10). In particular, we point the clear threshold behavior of the Born term as noted also by the authors of Refs. [31, 32, 33].

5. Effect of the finite quark and gluon widths on the QGP radiation

Finally, we calculate the QGP dilepton rate, taking into account not only the finite masses of the partons, but also their *broad spectral functions*, i.e. finite widths. For this purpose, we convolute the off-shell cross sections obtained in section 3 with $dN/d\sqrt{s}$ and with the spectral functions $A(m)$ in line with the equation (12) and (34).

The partonic spectral functions are related to the imaginary part of the trace of the effective propagator D^μ_μ and to the partonic self-energies Σ as follows:

$$A(p) = \frac{1}{\pi}\Im D^\mu_\mu(p) = -\frac{1}{\pi}\frac{\Im\Sigma(p)}{[p^2 - m^2_{current} - Re\Sigma(p)]^2 + [\Im\Sigma(p)]^2}. \qquad (32)$$

For the current analysis, we use the approximation of constant real and imaginary parts of the self-energy, which corresponds to constant finite average masses for quarks

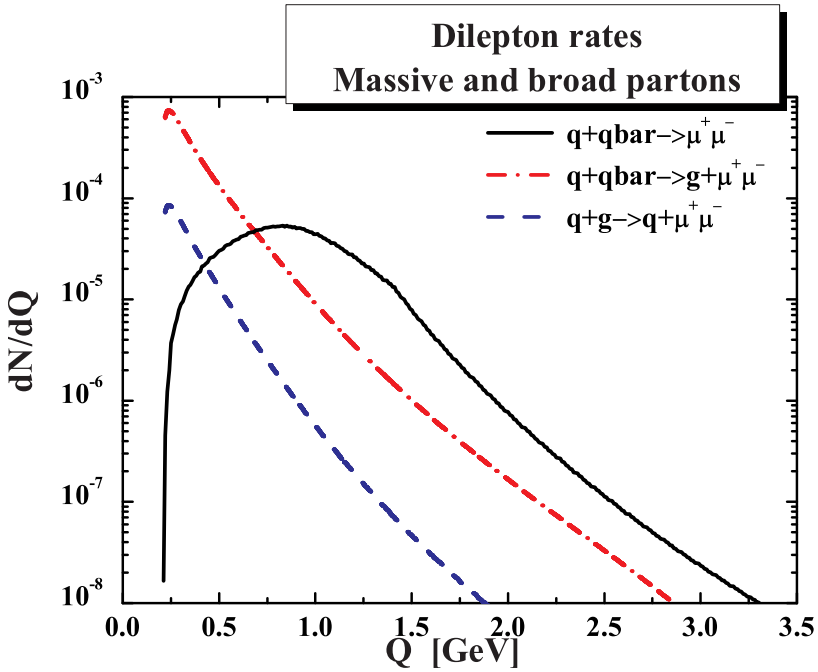

Figure 12. (color online) Dimuon rates from the QGP dN/dy beyond the on-shell approximation, $\alpha_S = 0.8$. The distribution dN/dQ calculated in the fully off-shell case of massive *and broad* dynamical quasi-particles. The rates are calculated using the off-shell cross sections convoluted with effective spectral functions of the Breit-Wigner type. The parameters of the spectral functions are: the peak of the quark spectral function is located at 0.3 GeV, the width is $\Gamma = 0.3$ GeV, the peak of the gluon spectral function is at 0.8 GeV, the width to $\Gamma = 0.3$ GeV.

$(< m_q >)$ and gluons (μ) and a constant widths for given temperature T. Within these approximations the spectral function has a Breit-Wigner form. The DQPM fit to lattice data suggests that the partonic widths at temperatures around $1.5-2\ T_c$ are of the order of 300 MeV [31].

The results of the numeric convolution of the off-shell cross sections with the spectral functions and with the $dN/d\sqrt{s}$ distribution are shown in Fig. 12 for realistic values of the spectral function parameters: the peak of the quark spectral function is located at 0.3 GeV, the width is $\Gamma = 0.3$ GeV, the peak of the gluon spectral function is at 0.8 GeV, the width $\Gamma = 0.3$ GeV. The rate from the Drell-Yan mechanism is shown by the solid black line, while the $Q(\alpha_S)$ $2 \to 2$ processes are displayed by the dashed blue and dash-dotted red lines. We have checked numerically that the rates for different values of the gauge parameter lie on top of each other.

By dressing the quark and gluon lines with effective spectral functions we model the effect of the quasi-particle interaction, including their multiple scattering. One observes by direct comparison of the Fig. 11 and Fig. 12 that the effect of parton spectral function width on the dilepton rates is quite dramatic. In particular, the threshold of the Drell-Yan contribution is "washed-out". In this observation we confirm the results of [28]. On the other hand, the effect of the partonic width and/or of multiple scattering on the

$2 \to 2$ processes has not been known so far. Wether the predicted shape of the dilepton spectrum in Fig. 12 is realized remains to be answered in a forthcoming comparison to experimental data [86].

6. Summary and Outlook

In the present work we have derived the off-shell cross sections of dilepton production by the constituents of the strongly interacting quark-gluon-plasma in the reactions $q + \bar{q} \to l^+l^-$ (Drell-Yan mechanism), $q + \bar{q} \to g + l^+l^-$ (quark annihilation with the gluon Bremsstrahlung in the final state), $q(\bar{q}) + g \to q(\bar{q}) + l^+l^-$ (gluon Compton scattering), $g \to q + \bar{q} + l^+l^-$ and $q(\bar{q}) \to q(\bar{q}) + g + l^+l^-$ (virtual gluon decay, virtual quark decay) by dressing the quark and gluon lines in the perturbative diagrams with effective non-perturbative propagators. We extend previous calculations of the cross sections of dilepton production in partonic collisions by assigning finite masses to all parton lines and, more importantly, by going beyond the zero width approximation for initial and finite partons.

We have shown in Section 3 that finite quark and gluon masses not only screen the soft and collinear singularities and shift the kinematical thresholds, but also modify the magnitude as well as Q and q_T dependence of the cross sections of all the calculated processes compared to the leading twist perturbative results for massless partons. The modification is higher at low Q^2 and at the edges of the phase space.

Next, we have illustrated in Section 4 the application of the (off-shell) cross section to the calculation of the dilepton yield from the QGP, using factorization and phenomenological parametrizations for the number of $q + \bar{q}$ and $g + q$ collisions and Breit-Wigner parametrizations for the spectral functions of quarks and gluons. We have found that the width of quarks and gluons has a dramatic effect on the dilepton production. In particular, the threshold of the Born term at low Q^2 is smeared, while the contribution of the $2 \to 2$ processes to the rate is increased.

The cross sections obtained in this study will form the basis of a consistent calculation of the dilepton production in heavy-ion collisions at SPS and RHIC energies by implementing the partonic processes into the transport approach of the PHSD collaboration [86]. The comparison to the dilepton data of the NA60 and PHENIX Collaborations will open the possibility to study the relative importance of different processes in the dilepton production and guide us towards a better understanding of the properties of matter created in heavy-ion collisions.

Acknowledgements

The author acknowledges valuable discussions with E. Bratkovskaya, W. Cassing, J. Manninen, V. Begun and A. Toia and the financial support through the "HIC for

FAIR" framework of the "LOEWE" program.

[1] I. Tserruya, (2009), 0903.0415.
[2] R. J. Fries, B. Müller, and D. K. Srivastava, Phys. Rev. Lett. **90**, 132301 (2003).
[3] E. V. Shuryak, Sov. Phys. JETP **47**, 212 (1978).
[4] E. V. Shuryak, Phys. Lett. **B78**, 150 (1978), Sov.J.Nucl.Phys. **28** (1978) 408, Yad.Fiz. **28** (1978) 796.
[5] E. L. Feinberg, Izv. Akad. Nauk Ser. Fiz. **34**, 1987 (1970).
[6] E. L. Feinberg, Nuovo Cim. **A34**, 391 (1976).
[7] J. D. Bjorken and H. Weisberg, Phys. Rev. **D13**, 1405 (1976).
[8] J. Cleymans, J. Fingberg, and K. Redlich, Phys. Rev. **D35**, 2153 (1987).
[9] NA60, R. Arnaldi *et al.*, Phys. Rev. Lett. **96**, 162302 (2006).
[10] NA60, J. Seixas *et al.*, J. Phys. **G34**, S1023 (2007).
[11] NA60, S. Damjanovic *et al.*, Nucl. Phys. **A783**, 327 (2007).
[12] R. Rapp, J. Wambach, and H. van Hees, (2009), 0901.3289.
[13] O. Linnyk, E. L. Bratkovskaya, and W. Cassing, Nucl. Phys. **A830**, 491c (2009).
[14] O. Linnyk, E. L. Bratkovskaya, and W. Cassing, (2010), 1001.3858.
[15] W. Cassing and E. L. Bratkovskaya, Phys. Rept. **308**, 65 (1999).
[16] E. L. Bratkovskaya, W. Cassing, and O. Linnyk, Phys. Lett. **B670**, 428 (2009).
[17] PHENIX, A. Toia, Nucl. Phys. **A774**, 743 (2006).
[18] PHENIX, A. Toia, Eur. Phys. J. **C49**, 243 (2007).
[19] PHENIX, S. Afanasiev *et al.*, (2007), 0706.3034.
[20] PHENIX, A. Adare *et al.*, (2009), 0912.0244.
[21] J. Manninen, E. L. Bratkovskaya, W. Cassing, and O. Linnyk, (2010), 1005.0500.
[22] F. Halzen and D. M. Scott, Phys. Rev. **D18**, 3378 (1978).
[23] Z.-w. Lin and C. M. Ko, Nucl. Phys. **A671**, 567 (2000).
[24] F. Halzen and D. M. Scott, Phys. Rev. Lett. **40**, 1117 (1978).
[25] L. D. Landau and I. Pomeranchuk, Dokl. Akad. Nauk Ser. Fiz. **92**, 535 (1953).
[26] L. D. Landau and I. Pomeranchuk, Dokl. Akad. Nauk Ser. Fiz. **92**, 735 (1953).
[27] A. B. Migdal, Phys. Rev. **103**, 1811 (1956).
[28] P. Aurenche, F. Gelis, G. D. Moore, and H. Zaraket, JHEP **12**, 006 (2002).
[29] F. Karsch, E. Laermann, P. Petreczky, S. Stickan, and I. Wetzorke, Phys.Lett. **B530**, 147 (2002).
[30] M. I. Gorenstein and O. A. Mogilevsky, Phys. Lett. **B228**, 121 (1989).
[31] W. Cassing, Nucl. Phys. **A795**, 70 (2007).
[32] A. Peshier, B. Kämpfer, O. P. Pavlenko, and G. Soff, Phys. Lett. **B337**, 235 (1994).
[33] M. H. Thoma, S. Leupold, and U. Mosel, Eur. Phys. J. **A7**, 219 (2000).
[34] L. D. McLerran and T. Toimela, Phys. Rev. **D31**, 545 (1985).
[35] E. Shuryak, Prog. Part. Nucl. Phys. **53**, 273 (2004).
[36] M. H. Thoma, J. Phys. **G31**, L7 (2005).
[37] A. Peshier and W. Cassing, Phys. Rev. Lett. **94**, 172301 (2005).
[38] PHENIX, K. Adcox *et al.*, Nucl. Phys. **A757**, 184 (2005).
[39] STAR, J. Adams *et al.*, Nucl. Phys. **A757**, 102 (2005).
[40] BRAHMS, I. Arsene *et al.*, Nucl. Phys. **A757**, 1 (2005).
[41] PHOBOS, B. B. Back *et al.*, Nucl. Phys. **A757**, 28 (2005).
[42] F. Karsch, Nucl. Phys. **A698**, 199 (2002).
[43] J. I. Kapusta, P. Lichard, and D. Seibert, Phys. Rev. **D44**, 2774 (1991).
[44] E. Braaten, R. D. Pisarski, and T.-C. Yuan, Phys. Rev. Lett. **64**, 2242 (1990).
[45] S. M. H. Wong, Z. Phys. **C58**, 159 (1993).
[46] R. D. Pisarski, Phys. Rev. Lett. **63**, 1129 (1989).
[47] V. P. Silin, Sov. Phys. J.E.T.P. **11**, 1136 (1960).
[48] V. V. Klimov, Sov. Phys. J.E.T.P. **55**, 199 (1982).

[49] H. A. Weldon, Phys. Rev. **D26**, 1394 (1982).
[50] R. Baier, M. Dirks, and K. Redlich, Acta Phys. Polon. **B28**, 2873 (1997).
[51] M. Strickland, Phys. Lett. **B331**, 245 (1994).
[52] J.-P. Blaizot and F. Gelis, Eur. Phys. J. **C43**, 375 (2005).
[53] F. Gelis, Nucl. Phys. **A715**, 329 (2003).
[54] W. Cassing, Nucl. Phys. **A791**, 365 (2007).
[55] R. Baier, B. Pire, and D. Schiff, Phys. Rev. **D38**, 2814 (1988).
[56] T. Altherr, P. Aurenche, and T. Becherrawy, Nucl. Phys. **B315**, 436 (1988).
[57] O. Linnyk, S. Leupold, and U. Mosel, Phys. Rev. **D71**, 034009 (2005), [Erratum-ibid. D **75**, 059901 (2007)].
[58] O. Linnyk, S. Leupold, and U. Mosel, Phys. Rev. **D75**, 014016 (2007).
[59] M. Schafer, H.C. Donges, A. Engel, and U. Mosel, Nucl. Phys. **A575**, 429 (1994).
[60] A. I. Titov, B. Kämpfer, and E. L. Bratkovskaya, Phys. Rev. **C51**, 227 (1995).
[61] R. Shyam and U. Mosel, Phys. Rev. **C79**, 035203 (2009); Phys. Rev. **C67**, 065202 (2003).
[62] L.P. Kaptari and B. Kampfer, Phys. Rev. **C80**, 064003 (2009); Nucl. Phys. **A764**, 338 (2006).
[63] E. L. Bratkovskaya, S. M. Kiselev, and G. B. Sharkov, Phys. Rev. **C78**, 034905 (2008).
[64] R. L. Jaffe, Lectures presented at the Los Alamos School on Quark Nuclear Physics, Los Alamos, N.Mex., Jun 10-14, 1985.
[65] E. V. Shuryak and A. I. Vainshtein, Nucl. Phys. **B199**, 451 (1982).
[66] A. A. Henneman, D. Boer and P. J. Mulders, Nucl. Phys. B **620** (2002) 331
[67] F. Eichstaedt, S. Leupold and U. Mosel, Phys. Rev. D **81** (2010) 034002
[68] C. J. Bomhof and P. J. Mulders, Nucl. Phys. B **795** (2008) 409
[69] S. D. Drell and T.-M. Yan, Phys. Rev. Lett. **24**, 181 (1970).
[70] G. Altarelli, G. Parisi, and R. Petronzio, Phys. Lett. **B76**, 351 (1978).
[71] A. I. Vainshtein, V. I. Zakharov, V. A. Novikov, and M. A. Shifman, JETP Lett. **24**, 341 (1976), [Pisma Zh. Eksp. Teor. Fiz. **24**, 376 (1976)].
[72] M. E. Peskin and D. V. Schroeder, *An Introduction to quantum field theory* (Reading, USA: Addison-Wesley, 1995).
[73] A. Kulesza and W. J. Stirling, J. Phys. G **26**, 637 (2000) [arXiv:hep-ph/9912300].
[74] A. Achilli, *et al* arXiv:0910.1867 [hep-ph].
[75] A. H. Compton, Phys. Rev. **21**, 483 (1923).
[76] A. H. Compton, Phys. Rev. **22**, 409 (1923).
[77] J. Collins and H. Jung, (2005), hep-ph/0508280.
[78] A. I. Akhiezer and V. B. Berestetsky, *Quantum electrodynamics (in Russian)* (Moscow: Nauka, 1981).
[79] T. H. West, Comp. Phys. Comm. **77**, 286 (1993).
[80] S. Wolfram, *The Mathematica Book, Fifth Edition* (Champaign, USA: Wolfram Media, 2003).
[81] F. Karsch, E. Laermann, and A. Peikert, Phys. Lett. **B478**, 447 (2000).
[82] V. V. Begun, M. I. Gorenstein, and O. A. Mogilevsky, (2010), 1001.3139.
[83] K. Redlich, Phys. Rev. **D36**, 3378 (1987).
[84] E. L. Bratkovskaya, and W. Cassing, Nucl. Phys. **A831** (2009) 215-242.
[85] O. Linnyk, E. L. Bratkovskaya, and W. Cassing, Int. J. Mod. Phys. **E17**, 1367 (2008).
[86] O. Linnyk, E. L. Bratkovskaya, and W. Cassing, *work in progress.*